Title: MEST inhibits ciliary sphingomyelin synthesis to promote tendon stem/progenitor cells osteochondrogenesis in traumatic heterotopic ossification

Authors: Bowen Lai[1†], Yuan Gao[1†], Jianquan Zhao[1], Zhilong Shen[2], Rui Gao[1], Heng Jiang[1*], Xuhui Zhou[1,3*]

Affiliations:

[1]Department of Orthopedics, Changzheng Hospital, Naval Medical University (Second Military Medical University); Shanghai, 200003, China.

[2]Department of Orthopedic Oncology, Changzheng Hospital, Naval Medical University (Second Military Medical University); Shanghai, 200003, China.

[3]Translational Research Centre of Orthopedics, Shanghai General Hospital, Shanghai Jiao Tong University School of Medicine; Shanghai, 200080, China.

*Corresponding author.

† These authors contributed equally to this work.

Email:

Bowen Lai (bwlaispine@smmu.edu.cn)

Yuan Gao (418987858@qq.com)

Jianquan Zhao (dr_zhaojq@163.com)

Zhilong Shen (shenzhilong2000@163.com)

Rui Gao (gaoruispine@126.com)

Heng Jiang (jiangheng81@outlook.com)

Xuhui Zhou (zhouxuhui@smmu.edu.cn)

Abstract: Traumatic heterotopic ossification (tHO) is a musculoskeletal disorder characterized by ectopic bone formation in soft tissues following trauma. However, the etiology and mechanisms of tHO remain unknown, and no treatments are highly effective for tHO. Here, by performing single-cell RNA sequencing (scRNA-seq) on two tHO mouse models, we found that

ciliary Hedgehog (Hh) and PI3K-Akt signaling in tendon stem/progenitor cells (TSPCs) is upregulated during tHO development, leading to the activation of GLI family zinc finger 2 (GLI2) transcription factor, which promotes mesoderm-specific transcript (MEST) gene expression. Untargeted lipidomics using liquid chromatography-tandem mass spectrometry (LC-MS/MS) on detached cilia indicated that MEST could reduce ciliary sphingomyelin (SM) levels by inhibiting SM synthesis in TSPCs, creating a positive feedback loop that amplified ciliary Hh signaling, enhancing TSPCs osteochondrogenesis and driving tHO formation. Targeting ciliary genes intraflagellar transport 88 (IFT88) or ADP ribosylation factor like GTPase 3 (ARL3) restored normal TSPCs osteochondrogenesis in vitro and attenuated ectopic bone formation in vivo by suppressing Hh and PI3K-Akt signaling. AAV-mediated MEST inhibition or exogenous SM administration in vivo also alleviates tHO progression. These findings may provide novel insights into tHO pathogenesis and potential therapeutic strategies.

Keywords: heterotopic ossification; primary cilia; tendon stem/progenitor cells; mesoderm-specific transcript; sphingomyelin

Main Text:

INTRODUCTION

Traumatic heterotopic ossification (tHO) is a common musculoskeletal disorder characterized by the formation of ectopic bone in soft tissues, affecting a significant proportion of patients who experience severe injuries or orthopedic procedures[1]. Although most cases of tHO present with localized symptoms such as pain, swelling, and restricted joint movement, severe cases can lead to significant functional impairments, including joint ankylosis and chronic disability, necessitating intensive surgical interventions like amputation[2]. However, the etiology and underlying biological mechanisms of tHO remain unknown. Notably, there are no effective drugs available that can specifically eliminate ectopic bone formation or decelerate the progression of tHO. Therefore, it is necessary to conduct more studies exploring the molecular mechanisms of tHO to provide new strategies for clinical treatment that alleviate the suffering of patients and the burden on medical resources.

Primary cilia are solitary, non-motile microtubule-based organelles that protrude from the cell surface, acting as essential sensory antennae for cells to receive and transduce extracellular signals[3]. They play crucial roles in various developmental and physiological processes, including

57 embryonic patterning, tissue homeostasis, and cellular differentiation[4]. Recent studies have
58 increasingly highlighted the involvement of primary cilia in skeletal biology. For instance,
59 primary cilia in osteocyte function as critical mechanosensors to maintain normal bone formation
60 and help to treat osteoporosis[5]. Our previous study found that primary cilia can positively
61 regulate the process of osteochondral differentiation of stem cells from patients with
62 fibrodysplasia ossificans progressiva (FOP), a genetic form of HO caused by gene point
63 mutations[6]. However, there is currently no research involving the function and regulatory
64 mechanisms of primary cilia in the pathogenesis of tHO.

65 The recruitment of stem/progenitor cells and their differentiation into osteoblasts or
66 chondrocytes are key steps in the formation of tHO[7]. Tendon stem/progenitor cells (TSPCs) are
67 located between the long and parallel collagen fiber chains of tendon and are surrounded by the
68 extracellular matrix[8]. TSPCs can differentiate into tenocyte tissue (tendon) and non-tenocyte
69 tissues (such as bone, cartilage, and adipose tissue) in different circumstances. Studies have
70 reported that the increased ectopic bone volume in Achilles tendon of rats is accompanied with
71 increased bone morphogenetic protein (BMP) expression and enhanced osteogenesis in TSPCs[9].
72 Moreover, the inhibition of the mTOR signaling by rapamycin treatment can suppress the
73 osteochondral differentiation of TSPCs and tHO[10]. Thus, it is important to explore whether
74 primary cilia regulate the abnormal osteochondrogenic differentiation in TSPCs and how
75 primary cilia contribute to the progression of tHO via specific mechanisms.

76 High-throughput sequencing technologies have been used to find potential mechanisms of
77 various diseases in recent years. In our study, we indicated that MEST might be a key
78 downstream molecule in the regulation of tHO by primary cilia by performing single-cell RNA
79 sequencing (scRNA-seq) in two tHO mouse models. MEST (mesoderm-specific transcript) is an
80 imprinted gene predominantly expressed from the paternal allele. The protein encoded by it is
81 widely expressed in mesodermal tissues (e.g., sclerotome-derived structures such as vertebrae,
82 ribs, and cartilage), belongs to the α/β hydrolase superfamily, and has enzymatic activity. A
83 study showed that knocking down MEST in human periodontal ligament stem cells will inhibit
84 the expression of their stem cell markers and proliferation ability and weaken their multi-lineage
85 differentiation (including osteogenesis and chondrogenesis) abilities[11]. MEST can also
86 upregulate mouse mesenchymal stem cells chondrogenesis along with miR-335-5p[12]. However,
87 no study focuses on whether MEST is involved in regulating TSPCs osteogenic or chondrogenic

88 differentiation. Therefore, it is necessary to explore the role of MEST in the development of tHO
89 and the possibility of targeting MEST as a novel therapeutic strategy.
90 There is a diffusion barrier in the transition zone at the base of the primary cilia, which can
91 restrict the free movement of proteins and lipids in and out of the cilia, resulting in differences in
92 the composition of proteins and lipids on the ciliary membrane and the cytoplasmic membrane.
93 Under the stimulation of mechanical stress or chemical signals, the selective movement of
94 specific lipids in and out of the cilia can dynamically influence the function of receptors on the
95 ciliary surface and the activity of downstream signaling, thereby regulating cell proliferation and
96 differentiation[13]. The disruption of the homeostasis of ciliary lipids has been reported to be
97 associated with a variety of diseases, including Joubert syndrome[14], Meckel-Gruber syndrome[15],
98 nephronophthisis[16], and polycystic kidney disease[17]. Some studies have reported that
99 abnormalities in genes encoding key enzymes involved in cholesterol metabolism can lead to
100 defects in the formation of primary cilia in osteoblasts and in the differentiation of osteoblasts,
101 resulting in craniofacial malformation[18,19]. Since MEST has been found to possess the
102 characteristics of lipase, which can promote the hypertrophy of adipocytes and expand the
103 volume of adipose tissue[20], MEST may be involved in lipid metabolism in tHO. Exploring the
104 role of MEST in regulating TSPCs ciliary lipids may be of great significance for clarifying the
105 pathogenesis of tHO.

106 In this study, we used single-cell RNA sequencing (scRNA-seq) on two tHO mouse models:
107 1) burn/tenotomy in C57BL/6 mice; 2) cardiotoxin (CTX)-induced injury of tibial muscle in *Nse-*
108 *Bmp4* mice (overexpresses bone morphogenetic protein 4 (BMP4) under the control of neuron-
109 specific enolase (Nse) promoter). We demonstrated that the activity of ciliary Hh and PI3K-Akt
110 signaling of TSPCs is significantly upregulated during tHO development, leading to the
111 activation and nuclear translocation of the transcription factor GLI2, which promotes the
112 expression of the MEST gene. The upregulation of MEST expression reduces ciliary
113 sphingomyelin (SM) abundance by inhibiting SM synthesis, which in turn amplifies the
114 activation of the ciliary Hh signaling. This forms a positive feedback loop that significantly
115 enhances the osteochondrogenesis of TSPCs, thereby driving local ectopic bone deposition and
116 contributing to the development and progression of tHO. Moreover, knocking down ciliary gene
117 or suppressing Hh/PI3K-Akt signaling restored normal TSPCs differentiation. Inhibiting MEST

118 expression or exogenous SM administration in vivo also had great therapeutic effects on tHO.
119 Unraveling these mechanisms may enhance our understanding of the pathogenesis of tHO and
120 pave the way for the development of innovative and effective therapeutic approaches.

121 **RESULTS**

122 **1. Primary cilia in stem/progenitor cells contribute to tHO progression**

123 To induce tHO by burn/tenotomy[21], 6- to 8-week-old male C57BL/6 mice were subjected to a
124 burn injury using a 60°C heated aluminum block on the dorsal skin, followed by resection of the
125 right Achilles tendon and subsequent experiments (Figure 1a). Tendon tissues from the injured
126 sites were harvested at 0 days (prior to injury), and at 3, 7, 21, and 56 days after injury for
127 subsequent histological examination (Figure 1b). H&E staining demonstrated disorganized and
128 irregular tendon fibrous tissue at 3 to 7 days post-injury. Chondrogenic structures were detected
129 at 21 days, and osteogenic structures were observed at 56 days. Masson trichrome staining
130 showed blue-stained tendon collagen fibers, with the progression of structural disorganization
131 and tHO being similar to that observed with HE staining. Von Kossa staining revealed the
132 appearance of brown calcified nodules at 21 days, which became deeply stained by 56 days,
133 suggesting calcium deposition due to new bone formation.

134 To explore the function of cilia in tHO, we performed immunofluorescence staining on
135 tendon tissues collected from mice at 0, 3, 7, 21, and 56 days post-injury (Figure 1c, S1a).
136 ARL13B, a specific marker for primary cilia, was used to quantify ciliated cells. The percentage
137 of ARL13B-positive cells was 27.21% in the control group (0 days post-injury). After injury, the
138 proportion of ARL13B-positive cells increased to 40.14% at 3 days, 38.07% at 7 days, and
139 44.42% at 21 days, before declining to 39.10% at 56 days (Figure S1b). These data indicated that
140 ciliated cells increased rapidly during tHO and may contribute to its development. To further
141 identify the potential specific cell types targeted by cilia in the process of tHO, double
142 immunofluorescence staining was performed on tendon tissue samples collected at various time
143 points post-injury (Figure 1c, S1a). The following marker pairs were used: ARL13B with CD31
144 (endothelial cells marker), ARL13B with F4/80 (macrophages marker), ARL13B with PDGFRα
145 (stem/progenitor cells marker), ARL13B with TNMD (tendon cells marker), and ARL13B with
146 α-SMA (smooth muscle cells marker). Immunofluorescence analysis revealed significant co-
147 localization between ARL13B and all five cell markers, with PDGFRα showing particularly
148 strong association (Figure 1c). Quantitative analysis demonstrated that the proportion of

149 ARL13B+PDGFRα+ double-positive cells was the highest among the five marker combinations
150 (Figure S1c). Specifically, the percentage of ARL13B+PDGFRα+ cells was 55.91% in the
151 control group, and this proportion significantly increased to 78.62% at 3 days, 85.56% at 7 days,
152 90.17% at 21 days, and 95.49% at 56 days after tHO injury (Figure S1b). We also found that
153 ARL13B is co-stained with both chondrogenic marker gene COL2A1 and osteogenic marker
154 gene OCN at 21 days and 56 days during tHO when osteochondrogenesis have occurred (Figure
155 1d, e). These data suggested that primary cilia may play a crucial role in tHO development,
156 potentially through their localization in stem/progenitor cells.

157 Single-cell RNA sequencing (scRNA-seq) can distinguish differences among individual cells
158 in a high-throughput manner, thereby clarifying cellular heterogeneity and underlying molecular
159 mechanisms during disease progression. Therefore, in our study, we reanalyzed a scRNA-seq
160 dataset of injured sites from burn/tenotomy mouse tHO model (GSE126060). The dataset
161 included 12 samples, with three samples per group at four time points: pre-injury (Day 0) and
162 post-injury (Day 3, Day 7, and Day 21). The UMAP plot showed a total of 21,880 cells detected
163 and divided into nine subclusters (Figure 2a) according to the previous study[22]. Bubble plot
164 revealed the marker genes of each cluster, and markers for the Mesenchymal cluster were Pdgfra
165 and Prrx1 (Figure 2b, c). Group-stratified UMAP plots revealed that, as tHO progresses, the
166 percentage of Macrophage cluster cells peaked at 3 days (74.43%) post-injury, later rapidly
167 reduced to 37.10% at 7 days and 15.02% at 21 days post-injury, indicating the evolution of the
168 local inflammatory phase (Figure 2d). In contrast, the Mesenchymal cluster cells exhibited a
169 larger proportion at 7 (43.44%) and 21 days (49.43%), suggesting that stem/progenitor cells
170 contributes greatly to tHO during this period (Figure 2d). Consequently, we analyzed the
171 differentially expressed genes in the Mesenchymal subcluster at 7 and 21 days post-injury
172 compared with the control group and revealed that 82 genes were upregulated in the
173 Mesenchymal subcluster at Day 7, and 53 genes were upregulated at Day 21 (Figure 2e).

174 Since the percentage of ciliated stem/progenitor cells greatly increased during tHO
175 development, we are interested in the expression of ciliary genes at single-cell level.
176 Intraflagellar transport protein 88 homolog (IFT88) functions as a core protein of the IFT-B
177 complex and drives anterograde transport within cilia. Many studies reported the role of IFT88 in
178 skeletal homeostasis[23] and bone diseases[24-27]. *Ift88* has low expression at single cell level likely
179 due to limited scRNA-seq depth, but still predominantly localizes to the Mesenchymal

180 subpopulation (Figure S2a, b), and shows a subtle upward trend during tHO (Figure S2c). We
181 then shifted our focus to another ciliary gene IFT20 which is also a component of the IFT-B
182 complex and has been reported to regulate ciliogenesis and skeletal development[28]. It can be
183 shown that *Ift20* are highly expressed in the Mesenchymal cluster (Figure 2f). Arf-like Protein 3
184 (ARL3), a small GTPase, is involved in ciliogenesis and the maintenance of ciliary function[29,30].
185 Specifically deleting ARL3 in muscle satellite cells impaired muscle hypertrophy, revealing its
186 potential role of regulating primary cilia in stem/progenitor cells. Indeed, *Arl3* mainly expressed
187 in Mesenchymal cluster in cells from tHO injured site (Figure 2f). Moreover, with the
188 development of tHO after injury, the expression of *Ift20* and *Arl3* in Mesenchymal cluster
189 rapidly increased in Day 7 and Day 21 group, while the trends over time were not significant in
190 other clusters (Figure 2g). qPCR analysis further demonstrated that the mRNA expression levels
191 of ciliary genes *Ift88, Ift20*, and *Arl3* had an increasing trend during tHO development and
192 peaked on Day 21 before slightly decreased on Day 56 (Figure S2d). We then explore the
193 expression of osteogenic (*Alpl*, *Runx2*, and *Bglap*) and chondrogenic (*Col1a1, Sox9*, and *Acan*)
194 genes during tHO development. scRNA-seq data showed these genes, especially chondrogenic
195 genes were mainly expressed in Mesenchymal cluster (Figure S2e) and showed increasing trends
196 during tHO progression with a higher expression in Day 7 and Day 21 after injury (Figure 1h).
197 qPCR analysis also showed the expression levels of osteogenic genes gradually increased and
198 reach the peaks at Day 56 (bone formation period) after injury (Figure 1i), while chondrogenic
199 genes peaked at Day 21 (cartilage formation period) and slightly reduced in Day 56 during tHO
200 progression (Figure 1j). These results indicated primary cilia and ciliary genes may mainly
201 functioned in stem/progenitor cells osteochondrogenesis during the progression of tHO.
202

203 **2. Inhibition of primary cilia alleviates TSPCs osteochondrogenesis and tHO**

204 Since the above results suggested that primary cilia on stem/progenitor cells may be involved
205 in tHO pathogenesis, and considering that abnormal differentiation of tendon stem/progenitor
206 cells (TSPCs) has been reported to potentially contribute to the pathogenesis of tHO[31,32], we
207 isolated TSPCs from the tendon tissues of C57BL/6 mice. Microscopic examination showed that
208 these TSPCs exhibited a fibroblast-like spindle-shaped morphology (Figure 3a). Flow cytometry
209 analysis demonstrated that 88.1% of the TSPCs were double-positive for Pdgfrα and Prrx1
210 (consistent with the scRNA-seq results), thereby confirming the stem/progenitor cell

211 characteristics of the isolated TSPCs (Figure 3a). Immunofluorescence staining for ARL13B and
212 Acetyl-α-Tubulin (AcTu) was used to observe changes of primary cilia in TSPCs following
213 knockdown of ciliary genes IFT88 and ARL3 using letivirus-shRNA (*shIft88* and *shArl3*). The
214 results showed a significant reduction in cilia counts and length (Figure 3b). Quantitative
215 analysis revealed that the proportion of ciliated TSPCs was approximately 53.54% in the control
216 group but decreased to 19.36% in the *shIft88* group and 34.70% in the *shArl3* group, indicating a
217 marked decrease in cilia number in TSPCs following ciliary gene knockdown (Figure 3c).
218 Additionally, the average cilia length was 3.37 μm in the control group but reduced to 2.06 μm
219 in the *shIft88* group and 2.14 μm in the *shArl3* group, demonstrating a significant shortening of
220 cilia length in TSPCs after ciliary gene knockdown (Figure 3d).
221 Previous studies have shown that the osteogenic and chondrogenic differentiation capabilities
222 of TSPCs are abnormally activated during the process of tHO, leading to the formation of ectopic
223 bone in tendon tissues[32]. Therefore, investigating whether cilia can regulate the TSPCs
224 osteochondrogenesis is important for exploring the regulatory mechanisms of cilia in tHO. We
225 first induced osteogenic differentiation in TSPCs and performed alizarin red staining. Compared
226 with the control group, the alizarin red staining was lighter in the *shIft88* and *shArl3* groups,
227 indicating less calcium deposition (Figure 3e, S3a). This suggests that knockdown of ciliary
228 genes attenuates the osteogenic differentiation capacity of TSPCs. qPCR analysis revealed that
229 the expression of osteogenesis-related genes *Alpl*, *Bglap*, *Run2* and *Sp7* was significantly
230 reduced in the *shIft88* and *shArl3* groups compared with the control group (Figure 3f). Similarly,
231 we induced chondrogenic differentiation in TSPCs with or without ciliary gene knockdown and
232 performed alcian blue staining. Compared with the control group, the alcian blue staining was
233 lighter in the *shIft88* and *shArl3* groups (Figure 3e, S3a). Meanwhile, qPCR analysis revealed
234 that the expression of chondrogenesis-related genes *Col2a1, Sox9* and *Acan* was significantly
235 reduced (Figure 3f). These findings identified a positive correlation between cilia function and
236 the osteochondrogenic differentiation capacity of TSPCs.
237 To locally inhibit ciliary function in vivo, we administered adeno-associated virus (AAV)
238 vectors carrying *shIft88* and *shArl3* via intramuscular injection into the lower limbs of mice with
239 tHO. The results showed that knockdown of *Ift88* and *Arl3* significantly decreased the bone
240 volume (BV) of ectopic bone formation, whereas bone mineral density (BMD) and trabecular
241 thickness (Tb.Th) was not significantly altered (Figure 3g, h). These results indicate that primary

242 cilia may positively modulate the osteogenic and chondrogenic differentiation of TSPCs, leading
243 to abnormal bone formation in local soft tissues and ultimately resulting in tHO, which could be
244 rescued by inhibition of ciliary function without influencing normal bone quality.
245
246 **3. Ciliary Hh and PI3K-Akt signaling are involved in tHO pathogenesis**
247 To further investigate the specific molecular mechanisms and downstream targets through
248 which primary cilia regulate tHO development, we conducted enrichment analysis on our
249 previously mentioned sequencing data. Gene Ontology (GO) enrichment analysis showed that
250 differentially expressed genes at the site of tHO 21 days post-injury were significantly enriched
251 in functions related to the extracellular matrix, ossification, and cartilage development (Figure
252 4a). Consistent with these findings, differentially expressed genes in TSPCs following
253 knockdown of ciliary genes were also enriched in skeletal system development, ossification, and
254 bone mineralization (Figure 4b). These results suggest a strong correlation between the
255 differentially expressed genes and tHO, indicating that targeting these genes may represent a
256 potential strategy for treating tHO. We further conducted Gene Set Enrichment Analysis (GSEA)
257 on the differentially expressed genes in TSPCs following knockdown of ciliary gene *Ift88*, and
258 the results showed significant enrichment and negative correlation (NES = -2.124) in the Hh
259 signaling pathway (Figure 4c). Given that the activity of the Hedgehog (Hh) signaling pathway is
260 dependent on the primary cilia for regulating embryonic development and tissue differentiation,
261 and considering that aberrant upregulation of Hh has been implicated in the pathogenesis of tHO
262 following injury[33], the Hh signaling activity within TSPCs cilia is likely closely related to tHO.
263 Additionally, KEGG enrichment analysis indicated that differentially expressed genes in the
264 Mesenchymal cluster of tHO tissues, as well as those in TSPCs following knockdown of ciliary
265 gene *Ift88*, were significantly enriched in the PI3K-Akt signaling pathway (Figure 4d, e).
266 To verify the bioinformatics analysis results, we performed qPCR analysis and found that the
267 mRNA expression of Hh signaling molecules *Shh* and *Ptch1* was significantly downregulated in
268 TSPCs undergoing osteogenic and chondrogenic differentiation after *shIft88* or *shArl3* treatment
269 (Figure 4f). Western blot analysis also demonstrated a significant reduction in the protein
270 expression levels of SHH and PTCH1 (Figure 4g). Additionally, during TSPCs
271 osteochondrogenesis, the ratios of phosphorylated PI3K to total PI3K (p-PI3K/PI3K) and
272 phosphorylated AKT to total AKT (p-AKT/AKT) were significantly decreased following ciliary

273 gene knockdown (Figure 4g), indicating reduced phosphorylation of PI3K and AKT and the
274 inactivation of the PI3K-Akt signaling. Smoothened (SMO) is a key seven-transmembrane
275 receptor involved in Hh signaling and is inhibited by PTCH1 when Hh signaling is inactive.
276 Upon binding of the Hh ligand to PTCH1, the inhibitory effect of PTCH on SMO is alleviated,
277 thereby enabling the activation of SMO. Interestingly, scRNA-seq analysis showed that *Smo*
278 mainly expressed (Figure 4h) and increased over time in Mesenchymal cluster (Figure 4i) during
279 tHO progression, further demonstrating the Hh signaling was activated in tHO. Collectively,
280 these results suggest that the primary cilia of TSPCs may lead to aberrant activation of Hh and
281 PI3K-Akt signaling, thereby promoting TSPCs osteochondrogenesis and exacerbating tHO
282 development.
283
284 **4. Primary cilia modulate MEST expression to promote tHO**
285 To further identify key genes involved in tHO and their potential crosstalk with primary cilia,
286 we obtained bulk-RNA sequencing data and analyzed the differentially expressed genes (Figure
287 S4a) from a public database for mouse tHO tissues (GSE233201). We then integrated these data
288 with RNA sequencing results from TSPCs with ciliary gene *Ift88* knockdown and control groups
289 (Figure S4b) to identify common differentially expressed genes. Genes upregulated in the
290 Mesenchymal cluster at 7 and 21 days during tHO (GSE126060), genes upregulated in injured
291 tissue at 21 days of tHO (GSE233201), and genes downregulated in TSPCs with ciliary gene
292 *Ift88* knockdown were obtained respectively (Table S1). Venn diagram analysis identified three
293 common differentially expressed genes: MEST, PTN, and COL2A1 among these three datasets
294 (Figure 5a). COL2A1 is a key gene for chondrogenic differentiation, while PTN showed
295 insignificant differences after validation (Figure S5a-d). Thus, we focused on the role of the
296 MEST gene in tHO in subsequent studies.
297 scRNA-seq analysis revealed that *Mest* is predominantly expressed in the Mesenchymal
298 cluster (Figure S4c, d). Both qPCR and Western blot analyses demonstrated a significant
299 reduction in *Mest* RNA and protein expression following knockdown of the ciliary genes *Ift88* or
300 *Arl3* (Figure S4e, f). Moreover, scRNA-seq analysis showed that the expression of *Mest* in the
301 Mesenchymal cluster exhibits an upward trend with the progression of tHO (Figure S4g).
302 Consistently, immunohistochemical analysis of tendon tissues at various time points after
303 establishment of tHO further showed that MEST protein expression is progressively upregulated

304 during the tHO development (Figure S4h), suggesting that MEST may play a significant role in
305 the regulatory mechanisms of tHO. Notably, immunofluorescence staining showed no significant
306 co-localization between MEST and AcTu (Figure 5b), indicating that MEST likely functions
307 outside but not within the cilia in TSPCs to influence cilia function and thereby contribute to the
308 occurrence and progression of tHO.
309

310 **5. Targeting MEST inhibits TSPCs osteochondrogenesis and tHO formation**

311 As MEST is primarily not localized within the cilia of TSPCs, we explored how MEST can
312 regulate tHO in a cilia localization-independent manner. We constructed two small interfering
313 RNAs (siRNAs): *siMest-1* and *siMest-2*, to inhibit *Mest* gene expression in vitro. qPCR analysis
314 revealed a significant decrease in *Mest* expression following *siMest* intervention, confirming that
315 *siMest* can effectively suppress MEST function (Figure 5d). Alizarin red staining showed that the
316 *siMest* group exhibited lighter staining and fewer calcium nodules compared with the control
317 group during osteogenic differentiation induction (Figure 5c, S3b). Additionally, the expression
318 of osteogenesis-related genes *Alpl, Runx2* and *Bglap* was significantly reduced (Figure 5d).
319 Similarly, alcian blue staining during chondrogenic differentiation induction showed that,
320 compared with the control group, the *siMest* group exhibited lighter staining and reduced
321 chondrogenic capacity (Figure 5c, S3b). The expression of chondrogenesis-related genes *Col2a1*,
322 *Sox9* and *Acan* was also decreased (Figure 5d). Moreover, we divided the Mesenchymal cluster
323 to Mest-high and Mest-low subclusters based on the expression level of Mest in burn/tenotomy
324 tHO scRNA-seq dataset (Figure 5e). Though *Alpl, Sp7,* and *Col2a1* were not significantly
325 expressed between two subclusters probably because of their extreme low expression in single-
326 cell level (Figure S5e), the expression of *Runx2, Sox9,* and *Acan* were greatly higher in Mest-
327 high subcluster (Figure 5e). These findings indicated that alleviating MEST expression diminish
328 the osteochondrogenic differentiation capacity of TSPCs.

329 We further employed immunofluorescence staining with AcTu to label the cilia of TSPCs in
330 the control and *siMest* groups (Figure 5f). Quantitative analyses (Figure 4g) showed no
331 significant difference in cilia number (58.26% vs 53.11%), while cilia length was significantly
332 shorter in the *siMest* group compared with the control group (2.46 μm vs 3.48 μm). In addition,
333 we performed in vivo experiments by locally injecting a AAV vector carrying *shMest* into mice
334 with tHO to silencing *Mest* expression in local injured tissues. Micro-CT imaging revealed that

335 ectopic bone volume in the *shMest* group was significantly lower than that in the control group,
336 while bone mineral density remained largely unchanged (Figure 5h, i). Collectively, these results
337 suggest that MEST can regulate ciliary function and TSPCs osteochondrogenesis in a ciliary
338 localization-independent manner, while targeting MEST may serve as a potential method to
339 restore normal TSPCs osteochondrogenesis and treat tHO.
340

341 **6. Activation of MEST transcription by GLI2 mediates Hh signaling in tHO**

342 GLI2, a key transcriptional activator of the Hh signaling pathway, can translocate to the
343 nucleus upon Hh signal activation and induces the expression of downstream genes involved in
344 cell proliferation and differentiation. The sequence logo of GLI2 transcription factor was shown
345 and the JASPAR database predicts that the GLI2 can bind to the MEST gene promoter at
346 positions 904-916 (gtgaccacccagc) and 1698-1710 (tggaccacgcact), both with relative score > 0.8
347 (Figure 6a). Dual-luciferase reporter assays using pGL4.10 as vector demonstrated that GLI2 can
348 bind to the MEST promoter at both predicted sites, with overexpression of GLI2 significantly
349 increasing luciferase activity, thus indicating that GLI2 positively regulates MEST transcription
350 (Figure 6b). To further elucidate the regulatory role of the GLI2 transcription factor in tHO, we
351 performed immunohistochemistry on injured tendon tissues obtained from mice with tHO and
352 found that GLI2 expression progressively increased during tHO development (Figure 6c).
353 Meanwhile, qPCR and Western blot analyses revealed that, compared with the control group, the
354 *Gli2* mRNA and protein expression levels of GLI2 were significantly downregulated with *shIft88*
355 or *shArl3* treatment during TSPCs osteochondrogenesis (Figure 6d, e). ChIP-qPCR assay further
356 demonstrated that GLI2 transcriptional factor could significantly bind to site 1/2 on MEST
357 promoter region (Figure 6f). To further investigate the role of GLI2 in regulating MEST
358 transcription, overexpression (GLI2-OE) and knockdown (*siGli2*) of Gli2 were performed in
359 TSPCs, affecting the Mest mRNA expression during both osteogenic and chondrogenic
360 differentiation, which further demonstrated that GLI2 activity was positively associated with
361 MEST gene transcription in TSPCs osteochondrogenesis (Figure 6g). Moreover, local injection
362 of AAV-*shMest* into tHO mice injured site decreased protein expression levels of SHH, GLI2,
363 PTCH1, and SMO, as shown by immunohistochemistry (Figure 6h). qPCR analysis also showed
364 reduced mRNA expression of Hh signaling molecules (*Shh, Ptch1, Gli2*, and *Smo)* in *shMest*
365 treated tHO mice (Figure 6i). Thus, the in vivo experiments indicated that targeting Mest may

366 alleviate the occurrence and progression of tHO by reducing the activation level of the Hh/Gli2
367 signaling. Collectively, these results suggested GLI2 as a positive regulator of MEST
368 transcription, while MEST in turn modulates GLI2 and Hh signaling activity during tHO
369 development.
370
371 **7. MEST regulates TSPCs osteochondrogenesis via Hh and PI3K-Akt signaling**
372 Previous results have confirmed that: 1) MEST can influence TSPCs osteochondrogenesis
373 and regulate tHO development in ciliary localization-independent manner; 2) GLI2 promote
374 MEST transcription during TSPCs osteochondrogenesis via Hh signaling; 3) Cilia-mediated Hh
375 and PI3K-Akt signaling play a crucial role in tHO pathogenesis. Thus, we became intrigued by
376 whether MEST regulates TSPCs osteochondrogenesis through Hh and PI3K-Akt signaling. We
377 first transfected *siMest* in TSPCs to knock down Mest gene expression in vitro. Compared with
378 *siNC* treated TSPCs, the expression levels of key Hh signaling molecules were downregulated at
379 both the mRNA (Figure 7a) and protein (Figure 7b) levels in *siMest* treated TSPCs during
380 osteogenic and chondrogenic differentiation. In addition, the phosphorylation levels of PI3K and
381 AKT were also decreased significantly (Figure 7c). These findings suggest that silencing Mest
382 expression can attenuate TSPCs osteochondrogenesis via Hh and PI3K-Akt signaling in tHO.
383 To further demonstrate whether: 1) The regulatory effects of primary cilia on TSPCs
384 osteochondrogenesis and tHO development is dependent on MEST activity; 2) Hh or PI3K-Akt
385 signaling is essential for MEST-induced hyperactivation of TSPCs osteochondrogenesis, we
386 performed rescue experiments in MEST overexpression (MEST-OE) TSPCs by targeting cilia or
387 Hh/PI3K-Akt signaling. Both osteogenic and chondrogenic differentiation were upregulated in
388 MEST-OE group, indicated by higher positive area of alizarin red and alcian blue staining
389 (Figure 7d, S3c). However, the effects can be significantly rescued by inhibiting cilia function
390 under *shIft88* treatment in MEST-OE TSPCs (Figure 7d, S3c), which reveals that primary cilia
391 promote TSPCs osteochondrogenesis by activating MEST. Targeting Hh and PI3K-Akt signaling
392 by GANT61 (GLI2 inhibitor) and LY294002 (PI3K inhibitor) respectively in MEST-OE TSPCs
393 also restored the normal osteochondrogenesis (Figure 7d, S3c), suggesting that Hh and PI3K-Akt
394 signaling serve as critical mediators through which MEST enhances TSPCs differentiation.
395 qPCR analysis showed consistent changes of osteogenesis (*Alpl, Runx2,* and *Bglap*) and
396 chondrogenesis (*Col2a1, Sox9,* and *Acan*) related genes expression with the staining results

397 under different treatment (Figure 7e). We also found that overexpression of MEST (MEST-OE)
398 lead to upregulated GLI2 (Figure S3d, 7f) and other Hh signaling molecules (*Shh, Ptch1*, and
399 *Smo*) expression (Figure 7g), as well as the phosphorylation levels of PI3K and AKT (Figure 7h),
400 which is opposite to the MEST knockdown effects during TSPCs osteochondrogenesis. These
401 findings add to evidence of the crucial role of Hh and PI3K-Akt signaling in MEST-regulated
402 TSPCs osteochondrogenesis and tHO development.
403 Since both Hh and PI3K-Akt signaling are involved in tHO pathogenesis, exploring the
404 relationship and crosstalk between them is of great significance. qPCR (Figure S3d) and western
405 blot (Figure 7f) showed that GANT61 (the specific inhibitor of GLI2 expression and GLI2-
406 mediated transcription) can reduced both GLI2 and MEST expression in MEST-OE TSPCs
407 during in vitro osteochondrogenesis. However, GANT61 cannot rescue the phosphorylation
408 levels of PI3K and AKT during MEST-OE TSPCs osteochondrogenesis (Figure 7h), while
409 LY294002 (PI3K inhibitor) can significantly attenuate the expression of GLI2/MEST (Figure
410 S3d, 7f) and Hh signaling molecules (Figure 7g), indicating that GLI2 and GLI2-regulated
411 MEST transcription is the downstream of PI3K/Akt signaling and the activation of GLI2-MEST
412 axis involved in TSPCs osteochondrogenesis can be inhibited by targeting PI3K/Akt signaling.
413
414 **8. MEST reduced ciliary sphingomyelin levels in TSPCs**
415 Recent studies have shown that ciliary lipids play a crucial role in maintaining ciliary
416 structure stability and regulating ciliary mechanosensation and signal transduction. Aberrant
417 distribution and dynamic changes in ciliary lipids have been implicated in various diseases,
418 including polycystic kidney disease[17] and obesity[34]. Moreover, deficiencies in key cholesterol-
419 metabolizing enzymes have been shown to cause ciliary defects that impact bone development[19].
420 These findings have prompted our interest in investigating the changes in lipids within TSPCs
421 cilia during tHO. We first isolated cilia from TSPCs in the control and *siMest* groups using
422 ultracentrifugation to prepare ciliary suspensions as previously reported[35] (for more details see
423 Methods). Immunofluorescence showed almost no cilia was left after isolation in non-ciliated
424 TSPCs (Figure 8a). Immunoblot further revealed ciliary enrichment of AcTu and absence of
425 cytoplasmic components (β-actin) in TSPCs cilia (Figure 8b), confirming that the cilia were
426 effectively removed from TSPCs without detectable components of cytoplasm. Then we
427 conducted untargeted lipidomics using liquid chromatography-tandem mass spectrometry (LC-

428 MS/MS) on the collected ciliary suspensions. OPLS-DA analysis showed obvious differences in
429 the lipid profiles of TSPCs cilia between the *siNC* and *siMest* groups (Figure 8c). We performed
430 differential analysis of lipids based on the LIPID MAPS® classification system and the
431 differential expressed primary (Figure 8d, e) and secondary (Figure S6a) lipids were classified.
432 Totally, we screened 159 upregulated and 157 downregulated lipids in the *siMest* group with the
433 criteria of |log2FC| > 1 and P value < 0.05 (Table S2, Figure 8f, S6b). Compared with the *siNC*
434 group, the abundance of sphingomyelin (SM) within the cilia of TSPCs in the *siMest* group was
435 significantly increased, while the content of triglycerides (TG) was significantly decreased
436 (Figure 8g). Heatmaps revealed consistent differential changes in almost all subclasses of SM
437 and TG, including 22 types of SM and 53 types of TG (Figure S6c). Other sphingolipids except
438 for SM also differentially expressed (mostly upregulated) in *siMest* group (Figure S6d). We also
439 conducted KEGG enrichment analysis to find the key lipid signaling involved in *siMest* TSPCs.
440 Consistent with our prior findings, the differentially expressed metabolites were enriched in
441 pathways including glycerophospholipid metabolism, sphingolipid signaling, and sphingolipid
442 metabolism (Figure 8h, S6e). Since SM is the most abundant sphingolipid and exhibits the most
443 significant difference before and after *siMest* knockdown, we then concentrate on the role of
444 ciliary SM metabolism in tHO pathogenesis.
445 SGMS2 (sphingomyelin synthase 2) gene encodes sphingomyelin synthase 2, which is
446 mainly involved in the synthesis of SM on the cell membrane. It has been reported that SGMS2-
447 mediated SM metabolism was involved in skeletal homeostasis regulation and its mutation could
448 lead to a series of bone diseases like osteoporosis and skeletal dysplasia[36]. We found that *Sgms2*
449 was mainly expressed in Mesenchymal cluster but rarely expressed in Mest-high subcluster,
450 while the expression level of *Sgms2* in Mest-high subcluster gradually reduced over time after
451 tHO at single-cell level (Figure 8i, j), indicating that MEST may reduce ciliary SM synthesis in
452 tHO by inhibiting Sgms2 expression. Moreover, qPCR (Figure 8k) and Western blot (Figure 8l)
453 demonstrated that the mRNA and protein expression levels of SGMS2 significantly increased
454 after *siMest* treatment during TSPCs osteogenesis and chondrogenesis. scRNA-seq analysis
455 demonstrated a subtle decrease in SM biosynthetic gene expression during tHO development,
456 while SM catabolic genes showed no significant expression changes (Figure 8m). These results
457 indicated that MEST may reduce the synthesis and abundance of SM within the cilia of TSPCs in

458 tHO progression, and that silencing *Mest* expression can promote SM synthesis by upregulating
459 SGMS2 activity and reverse the reduction of ciliary SM levels in TSPCs.
460
461 **9. Targeting ciliary sphingomyelin attenuates tHO development**
462 Since previous findings have demonstrated that MEST can activate TSPCs
463 osteochondrogenesis in ciliary localization-independent manner, thereby promoting the
464 occurrence and development of tHO, it is essential to explore whether ciliary lipids of TSPCs
465 also contribute to tHO pathogenesis. Research has shown that sphingomyelin and cholesterol
466 interact on the cellular membrane to regulate intracellular signaling processes, and their dynamic
467 balance is crucial for maintaining normal cellular functions[37]. Thus, exploring how MEST-
468 mediated sphingomyelin changes regulate TSPCs function is of great significance in tHO
469 pathogenesis. We induced osteogenic and chondrogenic differentiation in TSPCs and performed
470 alizarin red (ARS) and alcian blue (AB) staining with different treatments respectively (Figure
471 9a, b). Compared with the control group, treatment with exogenous sphingomyelin significantly
472 reduced the staining intensity and area, indicating that sphingomyelin can suppress TSPCs
473 osteochondrogenesis. Conversely, treatment of TSPCs with myriocin (a sphingomyelin synthesis
474 inhibitor) significantly enhanced TSPCs osteochondrogenesis. However, when sphingomyelin
475 and myriocin were applied together, the ARS or AB staining intensity and area were not
476 significantly different from the control group. Furthermore, downregulation of *Mest* gene
477 expression in TSPCs using *siMest* rescued the excessive upregulation of osteochondrogenesis
478 induced by myriocin treatment in TSPCs. qPCR analysis of the expression of osteogenic (*Alpl,*
479 *Runx2,* and *Bglap*) and chondrogenic (*Col2a1, Sox9,* and *Acan*) differentiation-related genes in
480 TSPCs revealed trends consistent with the staining results (Figure 9c), suggesting that inhibiting
481 *Mest* gene expression may increase ciliary sphingomyelin level in TSPCs, thereby attenuating
482 their osteogenic and chondrogenic differentiation capacities and alleviating tHO severity.
483 Notably, a study has demonstrated that depletion of sphingomyelin on ciliary membrane can
484 increase the accessibility of cholesterol, thereby amplifying the transmission of the Hh signaling
485 pathway within the cilia[38]. Therefore, we hypothesize that the results may be associated with the
486 activity of the Hh signaling pathway. Smoothened (SMO), a seven-transmembrane receptor
487 protein, serves as a bridge between Hh ligands and GLI transcription factors in the Hh pathway.
488 Direct targeting of SMO has become a trending area in drug research targeting the Hh signaling

489 pathway, with the SMO inhibitor vismodegib being FDA-approved for the treatment of basal cell
490 carcinoma[39]. When vismodegib was administered to TSPCs treated with myriocin, the ARS or
491 AB staining intensity and area was significantly reduced (Figure 9a, b), and the expression of
492 osteogenic (*Alpl, Runx2,* and *Bglap*) and chondrogenic (*Col2a1, Sox9,* and *Acan*) differentiation-
493 related genes was downregulated, with no significant differences compared to the control group
494 (Figure 9c). qPCR analysis of key Hh signaling molecules (*Shh, Ptch1, and Gli2*) during TSPCs
495 osteogenesis (Figure 9d) or chondrogenesis (Figure 9e) showed that myriocin strongly activated
496 Hh signaling during in vitro TSPCs differentiation, while exogenous sphingomyelin had the
497 opposite effect, inhibiting Hh signaling. In contrast, groups treated with myriocin +
498 sphingomyelin, myriocin + *siMest*, and myriocin + vismodegib exhibited Hh signaling gene
499 expression levels that were not significantly different from the control group (Figure 9d).
500 We also performed in vivo experiments by local injection of 1 mg/kg exogenous
501 sphingomyelin (SM) or 1X PBS (as the control group) into tHO mice injury site two times a
502 week for 8 weeks, resulting in a significantly reduced volume of ectopic bone in tHO mice after
503 SM treatment, with no significant differences in bone mineral density (Figure 9f). qPCR analyses
504 also showed reduced mRNA expression of Hh signaling molecules *Shh, Ptch1, Gli2*, and *Smo* in
505 *SM* treated tHO mice (Figure 9g). These findings suggest that the depletion of ciliary
506 sphingomyelin may facilitate the osteogenic and chondrogenic differentiation of TSPCs through
507 the activation of the Hh signaling, thereby exacerbating tHO progression. This effect can be
508 attenuated by silencing MEST gene expression or using SMO inhibitor vismodegib, which may
509 represent emerging candidate therapeutic targets for tHO.
510
511 **10. scRNA-seq on injured muscle from Nse-Bmp4 tHO model mice**
512 To further validate our findings and enhance the reliability of the results, we reanalyzed the
513 scRNA-seq data (GSE246445) on another tHO model mice which is performed by cardiotoxin
514 (CTX)-induced injury of tibial muscle in *Nse-Bmp4* mice[40].
515 After initial quality control, a total of 45287 cells of injured muscle from Nse-Bmp4 mice
516 were clustered into nine clusters based on the reported marker genes[40] (Figure 10a). While the
517 top two main cell types were skeletal muscle cells and MSC lineages, their proportion during
518 tHO development showed great changes. Notably, the percentage of MSC lineages increased
519 from 14.5% in uninjured group to 66.8% in Day 7 (post injury) group which showed converse

520 trend compared to the skeletal muscle cells (Figure 10b). Consistent with our findings, *Mest* was
521 mainly expressed in MSC lineages (Figure 10c) and showed an increasing expression in injured
522 muscle of *Nse-Bmp4* mice during tHO development (Figure 10d), especially expressing in
523 60.41% cells in Day 7 group (mainly in MSC lineages). These results demonstrated a significant
524 role of MEST from MSC lineages in tHO pathogenesis which supported our prior findings.
525 Moreover, we analyzed the significant differentiated expressed genes (DEGs) specifically in
526 MSC lineages among four groups (four different timepoints post injury) during tHO
527 development. The top10 higher variable genes in each group were shown by heatmap (Figure
528 10e). Chondrogenesis-related genes Acan and Col2a1 were top 2 DEGs in Day 7 group, which
529 showed the important role of MSC chondrogenesis in tHO, consistent with our results. GO and
530 KEGG enrichment analysis of DEGs in MSC lineages Day7 group (Figure 10f) also had several
531 common terms with the previous sequencing results shown in Figure 6, indicating that MSC
532 osteochondrogenesis was the key biological process in tHO progression.
533 Since we have found the potential role of primary cilia and cilia genes in tHO, we were
534 interested in the cilia genes expression in *Nse-Bmp4* tHO model mice at the single-cell level. A
535 total of 686 known cilia genes were obtained from the Syscilia Gold Standard[41]. Meanwhile, we
536 have identified 668 DEGs in Day 7 group of MSC lineages compared with other groups. We
537 then intersected two gene sets and got 13 common genes (Figure 10g), which could be
538 considered as important cilia genes in MSC lineage during tHO development. The expression
539 trends of 13 common cilia genes in each cluster (Figure 10h) or four groups in MSC lineages
540 (Figure 10i) were visualized. Among the 13 genes, IFT20 is the IFT-B complex which also
541 showed increased expression in injured cite of burn/tenotomy tHO model mice as shown in
542 Figure 2 and S2. PTCH1, the key receptor of Hh signaling, was also involved in the 13 common
543 cilia genes, which was consistent with our abovementioned findings. Furthermore, *Sgms2*
544 expression in the MSC lineage cluster declined over time after injury in the Nse-Bmp4 tHO
545 model (Figure S5f), consistent with the results from burn/tenotomy model (Figure 8), implicating
546 ciliary sphingomyelin metabolism (synthesis) in tHO development. Thus, scRNA-seq analysis of
547 the injured muscle from *Nse-Bmp4* tHO mice further demonstrated our conclusions.

548 **DISCUSSION**

549 The formation of traumatic heterotopic ossification (tHO) is a complex process involving the
550 aberrant differentiation of various types of cells into osteogenic and chondrogenic lineages.

551 Primary cilia are microtubule-based, non-motile organelles that act as cellular antennae, sensing
552 and transducing extracellular signals to regulate various developmental and physiological
553 processes. Several studies have revealed the relationship between primary cilia and skeletal
554 diseases, including defects of skeletal development such as polydactyly[42] and craniofacial
555 abnormalities[18]. Our previous research found that primary cilia in skeletogenic cells is crucial for
556 BMP and ActA-mediated osteogenesis and chondrogenesis and thereby governs the development
557 of fibrodysplasia ossificans progressiva (FOP)[6]. In this study, we demonstrate that cilia function
558 is significantly upregulated during tHO, with an increased prevalence of ciliated cells in the
559 injury site, particularly among stem/progenitor cells. This observation aligns with previous
560 studies indicating that primary cilia are essential for tissue repair[25] and regeneration[43] but extends
561 our understanding by linking cilia activity directly to the pathogenesis of tHO.
562 Our study reveals that primary cilia positively modulate TSPCs osteochondrogenesis,
563 contributing to the development of tHO. Knockdown of ciliary genes *Ift88* and *Arl3* significantly
564 reduced the osteochondrogenic differentiation capacity of TSPCs and ectopic bone volume in
565 tHO mice. This finding is consistent with the established role of primary cilia in regulating
566 stem/progenitor cell functions. For examples, loss of Numb (a ciliary protein) in spinal neural
567 progenitors lead to reduced cerebellar size via ciliary Hh signaling in mice[44]. The Hh signaling
568 pathway, which is cilia-dependent, is known to be aberrantly activated in postnatal
569 skeletogenesis[45] and heterotopic ossification in osteoblast[46]. Meanwhile, inactivated PI3K-Akt
570 signaling after ciliary gene IFT80 deficiency results in decreased odontogenic differentiation in
571 dental pulp stem cells[47]. Our study further supports this by showing that ciliary gene knockdown
572 in TSPCs downregulates Hh signaling and inactivates PI3K-Akt signaling, leading to reduced
573 osteochondrogenesis. Other pathway like TGFβ/BMP signaling is also widely studied on both
574 primary cilia[3] and tHO[48]. Fibrodysplasia ossificans progressiva (FOP) is a genetic form of HO
575 caused by mutations in the BMP type I receptor gene activin A receptor type 1 (ACVR1), while
576 our previous study[6] demonstrated that primary cilia regulate aberrant osteochondrogenesis via
577 pathological BMP signaling in FOP. Whether ciliary BMP signaling are involved in tHO
578 pathogenesis should be further explored in future research. In summary, we suggested that
579 primary cilia may serve as a crucial regulatory hub, integrating signals that drive the aberrant
580 TSPCs osteochondrogenesis during tHO progression.

581 A significant contribution of our study is the identification of MEST as a core regulator of
582 tHO for the first time. MEST encodes protein that is widely expressed in mesoderm. As we know,
583 the mesoderm develops into the skin, muscle, bone, and other connective tissues in our body,
584 which indicate the potential role of MEST in skeletogenesis. Our scRNA-seq results showed that
585 MEST is predominantly expressed in stem/progenitor cells and is upregulated during tHO
586 progression. A recent study reported that MEST specifically expressed in mesenchymal cells and
587 induced bone formation during mouse digit tip regeneration[49]. In our study, scRNA-seq showed
588 that the expression levels of osteogenic and chondrogenic genes in Mest highly expressed
589 stem/progenitor cells were higher than Mest low expressed stem/progenitor cells. Moreover,
590 knockdown of MEST in TSPCs attenuated their osteogenic and chondrogenic differentiation
591 capacities, while *shMest* significantly alleviate severity of tHO in mice, indicating a pivotal role
592 of MEST in promoting tHO by regulating TSPCs differentiation. Interestingly, MEST can
593 regulate the cilia length but not counts in TSPCs though it has no co-localization with primary
594 cilia. However, the specific mechanism of how MEST act on cilia remains unknown. Additional
595 studies are needed to characterize how MEST modulates ciliary structural remodeling and
596 interacts with key ciliary functional components. Overexpressing MEST in *shIft88* TSPCs can
597 rescue TSPCs reduced osteochondrogenic abilities, suggesting the effects of primary cilia on
598 TSPCs osteochondrogenesis and tHO is dependent on MEST activity. This finding is innovative
599 as it uncovers a novel regulatory axis involving cilia and MEST, highlighting a potential
600 therapeutic target for tHO.
601 Our study elucidates the molecular mechanisms through which MEST regulates tHO. We
602 showed that silencing MEST can suppress Hh and PI3K-Akt signaling and attenuate TSPCs
603 osteochondrogenesis in vitro. Overexpression of MEST promote TSPCs osteochondrogenesis via
604 activating Hh and PI3K-Akt signaling, and the effect can be rescued by Hh or PI3K-Akt inhibitor.
605 Furthermore, we show that the GLI2 transcription factor, a key activator of the Hh pathway,
606 binds to and promotes MEST transcription. This finding is supported by previous studies
607 indicating that GLI2 is a master regulator of bone homeostasis[50] and that its activity is tightly
608 regulated by cilia function[51]. Taken together, this study indicated that GLI2 transcriptional factor
609 activates MEST transcription and increase its gene expression, which in turn enhances TSPCs
610 osteogenesis and tHO progression via Hh and PI3K-Akt signaling.

611 In the presence of external stimuli, the selective influx and efflux of specific lipids in
612 primary cilia can dynamically modulate cell functions[13]. This process is intricately linked to
613 adipogenesis[34] and diseases such as polycystic kidney disease[17]. Thus, another novel aspect of
614 our study is the investigation of ciliary lipid metabolism in TSPCs during tHO. By untargeted
615 lipidomic after isolation of primary cilia, we show that MEST regulates the abundance of various
616 important lipids within TSPCs cilia, especially with sphingomyelin levels being significantly
617 upregulated upon MEST knockdown. This finding is intriguing as sphingomyelins are known to
618 interact with cholesterol to regulate ciliary signaling processes[38]. Recent studies showed that
619 SGMS2 mediated SM synthesis is involved in pancreatic cancer[52] and atherosclerosis[53].
620 Meanwhile, it is worth noting that SGMS2 is associated with early-onset osteoporosis[54] and
621 skeletal dysplasia[36], indicating its potential role in bone diseases. Our findings first indicated that
622 SGMS2 expression and SM synthesis may be activated by MEST knockdown, resulting in the
623 increased ciliary SM levels in *siMest* treated TSPCs, which may provide novel insights into the
624 treatment of tHO. Further studies should further concentrate on the mechanism by which MEST
625 may regulate SM metabolism in cilia. To explore the translational value of targeted SM
626 metabolism in tHO, we demonstrated that exogenous sphingomyelin treatment inhibits TSPCs
627 osteochondrogenesis and reduce ectopic bone volume in tHO mice. This effect is mediated
628 through the ciliary Hh signaling, as evidenced by the activation of Hh signaling upon myriocin
629 treatment and its inhibition by exogenous sphingomyelin. Vismodegib, a SMO inhibitor
630 targeting Hh signaling, can also diminish osteogenesis and chondrogenesis of TSPCs. The levels
631 of other sphingolipids and glycerophospholipids were also partly affected in *siMest* treated
632 TSPCs, indicating that other ciliary lipids except SM can also be involved in tHO pathogenesis
633 and need further studies to validate. These findings provide a new perspective on the role of lipid
634 metabolism in tHO and suggest that targeting ciliary sphingomyelin levels may represent a
635 potential therapeutic strategy.
636 Several limitations should be acknowledged in the study. First, our study primarily focuses
637 on the role of primary cilia in TSPCs, while other cell types[55,56] involved in tHO (such as
638 endothelial cells, muscle satellite cells, mesenchymal stem cells, adipose-derived stem cells,
639 fibroblasts, and immune cells) were not extensively investigated. Future studies should explore
640 the cilia-dependent functions of these cells and their interactions with TSPCs during tHO.
641 Second, our in vivo experiments were limited to local injection of AAV vectors carrying *shRNA*,

642 which may not fully recapitulate the complex physiological environment of tHO. Further studies
643 using genetically modified animal models are needed to validate our findings. Third, while we
644 identified MEST as a key regulator of tHO, the detailed molecular mechanisms through which
645 MEST modulates sphingomyelin metabolism within cilia remain unclear. Future studies should
646 investigate the specific interactions between MEST and lipid metabolic enzymes and their
647 impact on cilia function as the regulator of tHO. Finally, we did not explore whether and how
648 ECM stiffness alters cilia and their downstream signaling in tHO though 1) mechanical stimuli
649 can regulate bone formation via ciliary mechanical transduction[57]; 2) results of bioinformatic
650 analyses (Figure 5) show ECM-related biological processes may play a crucial role in TSPCs
651 osteochondrogenesis or tHO formation. Future studies should clarify how ECM stiffness after
652 injury influence local ectopic bone formation through ciliary mechanotransduction in tHO.
653 The schematic diagram of the study is shown in Figure 11. Our study opens several avenues
654 for future research. First, since primary cilia also located in other cell types during tHO
655 development, further investigation into the role of primary cilia in other cell types involved in
656 tHO is warranted. This will provide a more comprehensive understanding of the cilia-mediated
657 molecular mechanisms underlying tHO progression. Second, exploring the therapeutic potential
658 of targeting cilia function or MEST expression in preclinical models of tHO is an important next
659 step. This could involve the development of small molecules or gene therapies aimed at
660 modulating cilia activity or inhibiting MEST function. Third, elucidating the detailed molecular
661 mechanisms through which MEST regulates sphingomyelin or other lipid metabolism within
662 cilia will provide new insights into the pathogenesis of tHO and identify potential therapeutic
663 targets. Finally, translating these findings into clinical applications will require rigorous
664 preclinical and clinical trials to assess the safety and efficacy of cilia-targeted therapies for tHO.

665 MATERIALS AND METHODS

666 1. Experimental tHO mice

667 Male C57/BL6 mice weighing approximately 20 g and aged 6–8 weeks bought from
668 Hangzhou Ziyuan Laboratory Animal Technology Co., Ltd were used for construction of
669 burn/tenotomy tHO mice model as previously reported[21]. Briefly, mice were anesthetized via
670 intraperitoneal injection of sodium pentobarbital. Hair was removed from the left hind limb
671 (from the knee to the ankle) and a 2×3 cm area on the left side of the midline of the spine using
672 an electric clipper for surgical preparation. A longitudinal incision was made along the Achilles

673 tendon to expose the gastrocnemius tendon, which was then transected transversely. The skin
674 was sutured using 5-0 surgical thread. Subsequently, a 2×3×3 cm aluminum block preheated to
675 60°C in a water bath was applied to the 2×3 cm area on the left side of the midline of the spine
676 for approximately 17 seconds without additional pressure. The surgical site was disinfected with
677 an alcohol swab postoperatively, and mice were housed individually. Antibiotics and analgesics
678 were administered as needed. The success of the tHO model was evaluated 8–10 weeks post-
679 surgery. Local injection of 1 mg/kg sphingomyelin (#HY-113498, MCE) and 1X PBS at the
680 same dose into the injured muscle in tHO mice were performed two times per week.
681
682 **2. Micro-CT**
683 After euthanasia, the lower leg and foot of the mice were harvested and fixed overnight at
684 4°C in 10% formalin solution. Subsequently, the samples were subjected to high-resolution
685 micro-CT using a SkyScan CT reconstruction software (Bruker Corporation). Three-dimensional
686 modeling and additional data analysis were performed using 3D.SUITE (Bruker Corporation).
687 The entire ectopic bone region of the specimen was selected as the region of interest (ROI) for
688 quantification of bone volume (BV). Additionally, the distal tibial epiphysis of the mouse was
689 selected as the ROI for quantification of bone mineral density (BMD) and trabecular thickness
690 (Tb.Th).
691
692 **3. Immunofluorescence**
693 For immunofluorescence staining of tissues and cells, samples were prepared by fixing in
694 4% paraformaldehyde at 4°C for 24 hours (tissues) or at room temperature for 15 minutes (cells).
695 Tissues were subsequently deparaffinized and rehydrated through gradient ethanol, while cells
696 were permeabilized with ice-cold methanol or 0.3% Triton X-100 (Solarbio Life Sciences) as
697 needed. Both tissues and cells were blocked with 10% normal goat serum or 1% BSA to reduce
698 nonspecific binding. Primary antibodies, raised in different host species, were applied and
699 incubated overnight at 4°C. After washing, fluorophore-conjugated secondary antibodies (#A-
700 11034, Thermo Fisher Scientific) were added and incubated for 1 hour at room temperature in
701 the dark. Nuclei were stained with DAPI for 10–15 minutes, followed by washing. Sections and
702 cells were mounted with an anti-fade medium and imaged using Nikon ECLIPSE Ni microscopic
703 system. Primary antibodies used in immunofluorescence are listed in Table S3.

704

705 **4. Histology and immunohistochemistry**

706 Following euthanasia, the tHO mice tendon tissues were collected and fixed in 4%
707 paraformaldehyde at 4°C for 24 hours. After three washes with PBS, the samples were
708 decalcified in 10% EDTA at 4°C for 21 days. The tissues were then embedded in paraffin, and
709 sagittal sections of the Achilles tendon were obtained via paraffin microtomy. Histological
710 staining was performed using hematoxylin and eosin (H&E), Masson's trichrome, and Von
711 Kossa staining to evaluate ectopic ossification in the Achilles tendon. The sections were
712 dehydrated in ethanol, mounted, and imaged using Nikon ECLIPSE Ni microscopic system.

713 For immunohistochemistry on paraffin-embedded sections, the slides were first
714 deparaffinized in xylene and rehydrated through a graded ethanol series. Endogenous peroxidase
715 activity was quenched with 3% hydrogen peroxide in methanol. Antigen retrieval was performed
716 by heating the sections in citrate buffer (pH 6.0) for 10 minutes at 95–100°C. Sections were then
717 blocked with 10% fetal bovine serum or 1% BSA for 1 hour at room temperature. Primary
718 antibodies were applied and incubated either for 1 hour at room temperature or overnight at 4°C,
719 followed by washing with PBS. Secondary antibodies (#Ab205718, abcam) were added and
720 incubated for 30 minutes at room temperature. For visualization, sections were developed with
721 DAB substrate and counterstained with hematoxylin. Finally, the sections were dehydrated,
722 cleared, and mounted with neutral gum for microscopic examination using Nikon ECLIPSE Ni
723 microscopic system. Primary antibodies used in immunohistochemistry are listed in Table S3.

724

725 **5. Isolation of TSPCs and cell culture**

726 The isolation of TSPCs was conducted as previously reported[58]. Briefly, 6- to 8-week-old
727 C57/BL6 mice were sacrificed, and their entire gastrocnemius tendons were aseptically harvested.
728 The tendons were washed three times with 1X PBS and finely minced using ophthalmic scissors.
729 The minced tissue was collected in a 15 ml centrifuge tube and digested with 3 ml of 3 mg/ml
730 collagenase type I (#SCR103, Sigma-Aldrich) at 37°C in a shaking incubator for 45 minutes.
731 The mixture was then centrifuged at 500 rpm for 5 minutes to remove the collagenase.
732 Subsequently, the pellet was resuspended in 3 ml of 2 U/ml dispase type II (#4942078001,
733 Roche) and digested at 37°C for another 45 minutes. After centrifugation at 500 rpm for 1
734 minute to remove the dispase, the cell pellet was resuspended in 3 ml of low-glucose DMEM

735 supplemented with 10% fetal bovine serum (FBS) and 1% penicillin/streptomycin. The cell
736 suspension was filtered through a 70 μm cell strainer into a 10 cm culture dish and supplemented
737 with 6-8 ml of complete culture medium. The medium was changed for the first time after 3 days
738 and then every other day. When the cells reached 80% confluence (7-10 days later), they were
739 passaged for further experimental use. The drugs or substances added to TSPCs and the
740 concentration in the cell experiment are listed below: 10 μM myriocin (#HY-N6798, MCE), 20
741 μM sphingomyelin (#HY-113498, MCE), 10 μM vismodegib (#HY-10440, MCE), 4 μM
742 GANT61 (#HY-13901, MCE), 20 μM LY294002 (#HY-10108).
743
744 **6. Flow cytometry**
745 Fluorescence-activated cell sorting (FACS) analysis of mouse TSPCs were performed
746 following the protocols of previous studies[31,59]. We first removed the red blood cells from the
747 TSPCs using RBC Lysis Buffer (#46232, CST) and resuspend the cells in FACS buffer (1X PBS
748 + 2% FBS + 1mM EDTA). The extracted TSPCs were stained with antibodies for 30 min at 4°C
749 in the dark. Cells were then washed twice with FACS buffer to remove unbound antibodies.
750 Flow cytometry was performed using BD FACSAria™ III. Data were analyzed using BD FACS
751 Diva software and FlowJo software.
752
753 **7. Plasmid construction and transfection**
754 The pLVX-shRNA-puro lentivirus vector carrying shRNA was constructed by Shanghai
755 OBiO Technology Inc. for targeted gene knockdown in vitro. For lentivirus-mediated
756 transduction in TSPCs, 8×10^4 cells were seeded into each well of a 6-well plate. When the cell
757 density reached 20%–30%, cells were transduced with lentivirus in the presence of polybrene (8–
758 10 hours). Subsequently, stable transduced cells were selected using 2 μg/ml puromycin for 5–10
759 days. The successful establishment of stable cell lines was verified by quantitative qPCR and
760 Western blot (Figure S7a).
761 The pAAV-U6-shRNA-CMV-MCS-WPRE adeno-associated virus (AAV) vector carrying
762 shRNA was constructed by Shanghai OBiO Technology Inc. for targeted gene knockdown in
763 vivo. The shRNA sequences used are listed in Table S4. Forty-eight hours after tHO induction in
764 mice, 10 μL of the AAV was injected intramuscularly into the medial side of the injured hind
765 limb. Subsequent injections were administered every 3–5 days to achieve sustained knockdown

766 of the specific gene expression. The successful establishment of gene knockdown was verified
767 by quantitative qPCR and Western blot (Figure S7b, c).
768 The pCDNA3.1 plasmid carrying the full-length cDNA of Gli2 or Mest was constructed for
769 targeted gene overexpression in vitro. When cells reached 50%-60% confluence, plasmid (Gli2
770 pcDNA3.1 plasmid, Mest pcDNA3.1 plasmid, or pcDNA3.1 control plasmid) transfection was
771 carried out using Lipofectamine 3000 (#L3000001, Invitrogen) according to the manufacturer's
772 protocol. The cell culture medium was refreshed 24h after transfection.
773
774 **8. siRNA transfection**
775 The siRNA sequences used are listed in Table S4. For siRNA transfection, 1×10^5 cells were
776 seeded into each well of a 6-well plate. When the cell density reached 50%, cells were
777 transfected with siRNA using Lipofectamine RNAiMAX (Invitrogen). Specifically, the siRNA
778 was mixed with Lipofectamine RNAiMAX and incubated at room temperature for 10 minutes.
779 The mixture was then added to cells cultured in Opti-MEM reduced-serum medium. After
780 incubation for 48–72 hours, cells were harvested for subsequent experiments.
781
782 **9. Induction of TSPCs osteogenic and chondrogenic differentiation**
783 To induce osteogenic differentiation of TSPCs, gelatin-coated 6-well plates were used to
784 promote cell attachment and growth. TSPCs were seeded at a density of 1×10^4 cells/cm^2 and
785 cultured in osteogenic induction medium containing 10 mM β-glycerophosphate, 50 μg/ml
786 ascorbic acid, and 100 nM dexamethasone. The medium was changed every 2-3 days to maintain
787 optimal conditions. Osteogenic differentiation was assessed by alizarin red staining after 2-3
788 weeks to visualize calcium deposits. Additionally, qPCR was performed to evaluate the
789 expression of osteogenesis related genes.
790 To induce chondrogenic differentiation of TSPCs, cells were seeded at a density of 1×10^4
791 cells/cm^2 on gelatin-coated 6-well plates and cultured in chondrogenic induction medium
792 containing 10 ng/ml transforming growth factor-β3 (TGF-β3), 100 nM dexamethasone, 50 μg/ml
793 ascorbic acid, and 10 mM β-glycerophosphate. The medium was refreshed every 2-3 days to
794 ensure optimal conditions for differentiation. Chondrogenic differentiation was assessed by
795 histological staining with alcian blue to detect glycosaminoglycans at 2-3 weeks. qPCR was also
796 performed to evaluate the expression of chondrogenic markers.

797

798 **10. Quantitative polymerase chain reaction (qPCR)**

799 To assess the mRNA levels of the target genes, total RNA was purified from TSPCs using
800 an RNA Easy Fast Tissue/Cell Kit (#DP451, TIANGEN). The extracted mRNA was reverse-
801 transcribed into cDNA using FastKing gDNA Dispelling RT SuperMix (#KR118, TIANGEN).
802 Quantitative PCR was performed using the ABI Step One Plus system (Applied Biosystems).
803 Each reaction mixture (final volume of 20 μL) contained 1 μL of total cDNA, Power SYBR
804 Green PCR Master Mix (#A57155, Invitrogen), and gene-specific primers. The PCR protocol
805 included an initial denaturation at 95°C for 10 minutes, followed by 45 cycles of 95°C for 20
806 seconds, 72°C for 30 seconds, and a final dissociation curve analysis from 60°C to 95°C at a
807 heating rate of 0.1°C per second. GAPDH was used as an internal control. Relative gene
808 expression was calculated using the $2^{-\Delta\Delta Ct}$ method. Primers used in the study are listed in Table
809 S5.

810

811 **11. Western blot**

812 To perform western blot analysis, proteins were extracted from cells by washing with PBS,
813 lysing in RIPA buffer (#R0278, Sigma-Aldrich) containing Protease & Phosphatase Inhibitor
814 Cocktail (#78441, Thermo Fisher Scientific), and sonicating on ice. The lysates were centrifuged
815 at 4°C to collect the supernatant, and protein concentrations were determined using a BCA
816 Protein Assay Kit (#P0011, Beyotime). Equal amounts of protein were denatured by heating in
817 SDS loading buffer, separated by SDS-PAGE, and transferred to PVDF or nitrocellulose
818 membranes. Membranes were blocked with 5% skim milk in TBST to reduce nonspecific
819 binding. Primary antibodies were applied overnight at 4°C, followed by washing and incubation
820 with secondary antibodies conjugated to horseradish peroxidase (#SA00001-2, Proteintech Inc.)
821 for 1 hour at room temperature. After additional washing, the membranes were developed using
822 Super ECL Detection Reagent (#36208ES60, YEASEN) and imaged with ChemiDoc XRS+ Gel
823 Imaging System (Bio-Rad). Band intensities were quantified using ImageJ software, and target
824 protein expression levels were normalized to those of the internal control. Primary antibodies
825 used in western blot are listed in Table S3.

826

827 **12. RNA-seq**

828 Total RNA was isolated from samples using RNA Easy Fast Tissue/Cell Kit (#DP451,
829 TIANGEN). The purity and concentration of the extracted RNA were assessed using the
830 NanoDrop One spectrophotometer (Thermo Fisher Scientific). RNA integrity was further
831 evaluated using the Agilent 2100 Bioanalyzer (Agilent Technologies). Subsequently, RNA
832 sequencing libraries were prepared using the VAHTS Universal V6 RNA-seq Library Prep Kit
833 (Vazyme). The transcriptome sequencing and subsequent bioinformatics analysis were
834 performed by Shanghai OE Biotech. Sequencing libraries were sequenced on the Illumina
835 Novaseq 6000 platform to generate 150-bp paired-end reads. The raw sequencing reads in
836 FASTQ format were processed using the fastp software to remove low-quality reads, yielding
837 clean reads for subsequent data analysis. The clean reads were aligned to the reference genome
838 using the HISAT2 software, and gene expression levels were calculated in terms of fragments
839 per kilobase of transcript per million mapped reads (FPKM). Additionally, read counts for each
840 gene were obtained using HTSeq-count. Subsequent analyses, including principal component
841 analysis (PCA), differential gene expression analysis, and enrichment analysis, were performed
842 using the R software.
843

844 **13. Untargeted lipidomics using liquid chromatography-tandem mass spectrometry (LC-**
845 **MS/MS)**

846 TSPCs were cultured in serum-free medium to promote cilium growth until confluence. The
847 cells were washed with PBS and subjected to shear force by rotating at 360 rpm in a shaking
848 incubator at 37°C for 4 minutes to detach cilia as previously reported[35]. The cell debris was
849 removed by centrifugation at 1000×g for 10 minutes at 4°C, followed by ultracentrifugation at
850 40,000×g for 30 minutes at 4°C to isolate the ciliary suspension from the supernatant. The ciliary
851 suspension was then used for untargeted lipidomics sequencing.
852 For lipid extraction, 200 μL of pre-chilled methanol/water (3:1, v/v) was added to the ciliary
853 suspension, followed by sonication on ice for 15 minutes. Then, 1 mL of pre-chilled methyl tert-
854 butyl ether (MTBE) was added and vortexed thoroughly. The mixture was rotated at 4°C for 1
855 hour, followed by sonication on ice for another 30 minutes. After adding 100 μL of water and
856 vortexing for 1 minute, the mixture was left at room temperature for 10 minutes. The sample was
857 then centrifuged at 14,000×g for 15 minutes at 4°C. The supernatant was collected, and the pellet
858 was dried under a stream of nitrogen. The dried pellet was re-dissolved in 200 μL of SDT buffer.

859 Protein concentration was measured using the BCA assay. Based on the protein content, the cell
860 quantity in each sample was estimated, and equal cell amounts were taken from each supernatant.
861 The supernatant was dried using a high-speed vacuum concentrator, re-dissolved in 60 μL of pre-
862 chilled isopropanol/methanol (1:1, v/v), and centrifuged at 20,000×g for 20 minutes at 4°C. The
863 supernatant was vortexed and transferred to an injection vial for analysis. The entire analysis was
864 performed at 4°C using an automatic sampler. The samples were analyzed using a SHIMADZU-
865 LC30 ultra-high-performance liquid chromatography (UHPLC) system equipped with an
866 ACQUITY UPLC® HSS C18 column (2.1×100 mm, 1.9 μm) (Waters, Milford, MA, USA). To
867 avoid signal drift, samples were analyzed in a random order. A quality control (QC) sample was
868 inserted every 5-10 experimental samples to monitor system stability and data reliability. The
869 samples were analyzed in both positive and negative ion modes using electrospray ionization
870 (ESI). After separation by UHPLC, the samples were analyzed using a QExactive Plus mass
871 spectrometer (Thermo Fisher Scientific). Lipid identification and quantification were performed
872 using the MSDIAL software (Version 5.2.240218.2-net472) with the following parameters:
873 precursor mass tolerance of 10 ppm, product mass tolerance of 10 ppm, retention time alignment
874 of 0.1 min, and peak area filtering to reduce false positives. Lipids with relative standard
875 deviations (RSD) exceeding 30% in QC samples were excluded. The data were normalized to the
876 total peak area, preprocessed with UV-scaling, and subjected to multivariate statistical analyses,
877 including unsupervised principal component analysis (PCA), supervised partial least squares
878 discriminant analysis (PLS-DA), and orthogonal partial least squares discriminant analysis
879 (OPLS-DA). Univariate statistical analyses included Student's t-test and fold-change analysis,
880 and volcano plots and hierarchical clustering were generated using R software.
881
882 **14. Dual-luciferase reporter assay**
883 The Dual-Luciferase Reporter Assay was performed using the Dual-Luciferase Reporter
884 Assay System (Promega). The firefly luciferase reporter gene was cloned downstream of the
885 wild-type (WT) or mutant (MUT) pGL4.10-Mest promoter regions and co-transfected into
886 TSPCs with pcDNA3.1-GLI2 and Renilla expression vector pRL-TK. Following a 48-hour
887 incubation, cell lysates were prepared, and firefly luciferase activity was quantified and
888 normalized to Renilla luciferase activity as an internal control.
889

890 **15. Chromatin immunoprecipitation (ChIP) assay**

891 The ChIP assay was performed according to the previous study[60] using Pierce™ Agarose ChIP
892 Kit (#26156, Thermo Fisher Scientific). In brief, TSPCs were fixed with 1% formaldehyde,
893 quenched with 1X glycine solution, and lysed using Lysis Buffer supplemented with protease
894 inhibitors. Chromatin was digested with ChIP-grade micrococcal nuclease. The digested
895 chromatin was incubated overnight at 4°C with GLI2 antibody in Dilution Buffer. ChIP-grade
896 Protein A/G Plus Agarose beads were added to each immunoprecipitation (IP), followed by
897 centrifugation and washing with Wash Buffer. Elution was performed using 150 μL IP Elution
898 Buffer, 6 μL 5 M NaCl, and 2 μL 20 mg/mL Proteinase K. DNA fragments were analyzed by
899 real-time PCR. The primer sequences for ChIP-qPCR were designed based on +/-150 bp of the
900 two predicted sites on MEST promoter region and provided in Table S5.

901

902 **16. Bioinformatics analysis**

903 The scRNA sequencing dataset from the GEO database (GSE126060 and GSE246445).
904 Dimensionality reduction, clustering, and cell-type identification of the scRNA sequencing data
905 were performed using the Seurat package in R software. Additionally, bulk RNA sequencing
906 data from the heterotopic ossification sites of mice three weeks post-trauma was also obtained
907 from the GEO database (GSE233201). Differential gene expression analysis was conducted
908 using the DESeq2 package, while enrichment analysis was performed with the clusterProfiler
909 package. Transcription factor binding sites were predicted using the JASPAR database
910 (https://jaspar.elixir.no/).

911

912 **17. Statistical analysis**

913 All statistical analyses were performed using SPSS software and R Studio. Data are
914 presented as mean ± standard deviation (SD) of three independent assays. Statistical analyses
915 were performed by Student's t-test for two-group comparison and one-way ANOVA analyses
916 with Tukey's post hoc test for multiple comparisons. Statistical significance was set at $P < 0.05$.

917 **List of Supplementary Materials**

918 Figure S1 to S7 for multiple supplementary figures

919 Table S1 to S5 for multiple supplementary tables (including Excel files)

References and Notes

1 Dey, D. *et al.* The traumatic bone: trauma-induced heterotopic ossification. *Transl Res* **186**, doi:10.1016/j.trsl.2017.06.004 (2017).

2 Ranganathan, K. *et al.* Heterotopic Ossification: Basic-Science Principles and Clinical Correlates. *The Journal of Bone and Joint Surgery. American Volume* **97**, 1101-1111, doi:10.2106/JBJS.N.01056 (2015).

3 Mill, P., Christensen, S. T. & Pedersen, L. B. Primary cilia as dynamic and diverse signalling hubs in development and disease. *Nature Reviews. Genetics* **24**, 421-441, doi:10.1038/s41576-023-00587-9 (2023).

4 Anvarian, Z., Mykytyn, K., Mukhopadhyay, S., Pedersen, L. B. & Christensen, S. T. Cellular signalling by primary cilia in development, organ function and disease. *Nature Reviews. Nephrology* **15**, 199-219, doi:10.1038/s41581-019-0116-9 (2019).

5 Spasic, M., Duffy, M. P. & Jacobs, C. R. Fenoldopam Sensitizes Primary Cilia-Mediated Mechanosensing to Promote Osteogenic Intercellular Signaling and Whole Bone Adaptation. *J Bone Miner Res* **37**, 972-982, doi:10.1002/jbmr.4536 (2022).

6 He, K. *et al.* Primary cilia mediate skeletogenic BMP and Hedgehog signaling in heterotopic ossification. *Sci Transl Med* **16**, eabn3486, doi:10.1126/scitranslmed.abn3486 (2024).

7 Hwang, C. D. *et al.* Contemporary perspectives on heterotopic ossification. *JCI Insight* **7**, doi:10.1172/jci.insight.158996 (2022).

8 Bi, Y. *et al.* Identification of tendon stem/progenitor cells and the role of the extracellular matrix in their niche. *Nat Med* **13**, 1219-1227 (2007).

9 Dai, G. *et al.* Higher BMP Expression in Tendon Stem/Progenitor Cells Contributes to the Increased Heterotopic Ossification in Achilles Tendon With Aging. *Front Cell Dev Biol* **8**, 570605, doi:10.3389/fcell.2020.570605 (2020).

10 Chen, Y. *et al.* Targeted pathological collagen delivery of sustained-release rapamycin to prevent heterotopic ossification. *Sci Adv* **6**, eaay9526, doi:10.1126/sciadv.aay9526 (2020).

11 Hasegawa, D. *et al.* MEST Regulates the Stemness of Human Periodontal Ligament Stem Cells. *Stem Cells Int* **2020**, 9672673, doi:10.1155/2020/9672673 (2020).

12 Lin, X. *et al.* MiR-335-5p promotes chondrogenesis in mouse mesenchymal stem cells and is regulated through two positive feedback loops. *J Bone Miner Res* **29**, 1575-1585, doi:10.1002/jbmr.2163 (2014).

13 Dutta, P. & Ray, K. Ciliary membrane, localised lipid modification and cilia function. *Journal of Cellular Physiology* **237**, 2613-2631, doi:10.1002/jcp.30787 (2022).

14 Chávez, M. *et al.* Modulation of Ciliary Phosphoinositide Content Regulates Trafficking and Sonic Hedgehog Signaling Output. *Developmental Cell* **34**, 338-350, doi:10.1016/j.devcel.2015.06.016 (2015).

15 Hakeem, A. & Yang, S. Regulation of INPP5E in Ciliogenesis, Development, and Disease. *International Journal of Biological Sciences* **21**, 579-594, doi:10.7150/ijbs.99010 (2025).

16 Garcia, H. *et al.* Agonists of prostaglandin E2 receptors as potential first in class treatment for nephronophthisis and related ciliopathies. *Proc Natl Acad Sci U S A* **119**, e2115960119, doi:10.1073/pnas.2115960119 (2022).

957 17 Ha, K. *et al.* Cilia-enriched oxysterol 7β,27-DHC is required for polycystin ion channel activation. *Nat*
958 *Commun* **15**, 6468, doi:10.1038/s41467-024-50318-9 (2024).
959 18 Iwaya, C., Suzuki, A. & Iwata, J. Loss of Sc5d results in micrognathia due to a failure in osteoblast
960 differentiation. *J Adv Res* **65**, 153-165, doi:10.1016/j.jare.2023.12.008 (2024).
961 19 Suzuki, A. *et al.* Disruption of Dhcr7 and Insig1/2 in cholesterol metabolism causes defects in bone
962 formation and homeostasis through primary cilium formation. *Bone Research* **8**, 1, doi:10.1038/s41413-
963 019-0078-3 (2020).
964 20 Nikonova, L. *et al.* Mesoderm-specific transcript is associated with fat mass expansion in response to a
965 positive energy balance. *FASEB Journal : Official Publication of the Federation of American Societies For*
966 *Experimental Biology* **22**, 3925-3937, doi:10.1096/fj.08-108266 (2008).
967 21 Peterson, J. R. *et al.* Direct Mouse Trauma/Burn Model of Heterotopic Ossification. *J Vis Exp*, e52880,
968 doi:10.3791/52880 (2015).
969 22 Huber, A. K. *et al.* Immobilization after injury alters extracellular matrix and stem cell fate. *The Journal of*
970 *Clinical Investigation* **130**, 5444-5460, doi:10.1172/JCI136142 (2020).
971 23 Sun, J. S. *et al.* Ventromedial hypothalamic primary cilia control energy and skeletal homeostasis. *The*
972 *Journal of Clinical Investigation* **131**, doi:10.1172/JCI138107 (2021).
973 24 Verbruggen, S. W. *et al.* A Novel Primary Cilium-Mediated Mechanism Through which Osteocytes
974 Regulate Metastatic Behavior of Both Breast and Prostate Cancer Cells. *Adv Sci (Weinh)* **11**, e2305842,
975 doi:10.1002/advs.202305842 (2024).
976 25 Chen, H. *et al.* The effects of primary cilia-mediated mechanical stimulation on nestin+-BMSCs during
977 bone-tendon healing. *J Adv Res*, doi:10.1016/j.jare.2024.09.012 (2024).
978 26 Coveney, C. R. *et al.* Ciliary IFT88 Protects Coordinated Adolescent Growth Plate Ossification From
979 Disruptive Physiological Mechanical Forces. *J Bone Miner Res* **37**, 1081-1096, doi:10.1002/jbmr.4502
980 (2022).
981 27 Zhou, J. *et al.* Sinusoidal Electromagnetic Fields Increase Peak Bone Mass in Rats by Activating
982 Wnt10b/β-Catenin in Primary Cilia of Osteoblasts. *J Bone Miner Res* **34**, 1336-1351,
983 doi:10.1002/jbmr.3704 (2019).
984 28 Noda, K., Kitami, M., Kitami, K., Kaku, M. & Komatsu, Y. Canonical and noncanonical intraflagellar
985 transport regulates craniofacial skeletal development. *Proc Natl Acad Sci U S A* **113**, E2589-2597,
986 doi:10.1073/pnas.1519458113 (2016).
987 29 Huang, Y. *et al.* ARL3 GTPases facilitate ODA16 unloading from IFT in motile cilia. *Sci Adv* **10**,
988 eadq2950, doi:10.1126/sciadv.adq2950 (2024).
989 30 Zhang, R.-K., Sun, W.-Y., Liu, Y.-X., Zhang, E. Y. & Fan, Z.-C. RABL2 promotes the outward transition
990 zone passage of signaling proteins in cilia via ARL3. *Proc Natl Acad Sci U S A* **120**, e2302603120,
991 doi:10.1073/pnas.2302603120 (2023).

992 31 Feng, H. *et al.* Tendon-derived cathepsin K-expressing progenitor cells activate Hedgehog signaling to
993 drive heterotopic ossification. *The Journal of Clinical Investigation* **130**, 6354-6365,
994 doi:10.1172/JCI132518 (2020).
995 32 Chen, S. *et al.* A CD26+ tendon stem progenitor cell population contributes to tendon repair and
996 heterotopic ossification. *Nat Commun* **16**, 749, doi:10.1038/s41467-025-56112-5 (2025).
997 33 Regard, J. B. *et al.* Activation of Hedgehog signaling by loss of GNAS causes heterotopic ossification. *Nat*
998 *Med* **19**, 1505-1512, doi:10.1038/nm.3314 (2013).
999 34 Yamakawa, D. *et al.* Primary cilia-dependent lipid raft/caveolin dynamics regulate adipogenesis. *Cell*
1000 *Reports* **34**, 108817, doi:10.1016/j.celrep.2021.108817 (2021).
1001 35 Raleigh, D. R. *et al.* Cilia-Associated Oxysterols Activate Smoothened. *Mol Cell* **72**,
1002 doi:10.1016/j.molcel.2018.08.034 (2018).
1003 36 Pekkinen, M. *et al.* Osteoporosis and skeletal dysplasia caused by pathogenic variants in SGMS2. *JCI*
1004 *Insight* **4**, doi:10.1172/jci.insight.126180 (2019).
1005 37 Luchetti, G. *et al.* Cholesterol activates the G-protein coupled receptor Smoothened to promote Hedgehog
1006 signaling. *ELife* **5**, doi:10.7554/eLife.20304 (2016).
1007 38 Kinnebrew, M. *et al.* Cholesterol accessibility at the ciliary membrane controls hedgehog signaling. *ELife* **8**,
1008 doi:10.7554/eLife.50051 (2019).
1009 39 Dlugosz, A., Agrawal, S. & Kirkpatrick, P. Vismodegib. *Nat Rev Drug Discov* **11**, 437-438,
1010 doi:10.1038/nrd3753 (2012).
1011 40 Kan, C. *et al.* Spatiotemporal Analysis of Mesenchymal Stem Cells Fate Determination by Inflammatory
1012 Niche Following Soft Tissue Injury at a Single-Cell Level. *Adv Sci (Weinh)* **11**, e2310282,
1013 doi:10.1002/advs.202310282 (2024).
1014 41 Vasquez, S. S. V., van Dam, J. & Wheway, G. An updated SYSCILIA gold standard (SCGSv2) of known
1015 ciliary genes, revealing the vast progress that has been made in the cilia research field. *Molecular Biology*
1016 *of the Cell* **32**, br13, doi:10.1091/mbc.E21-05-0226 (2021).
1017 42 Taylor, S. P. *et al.* Mutations in DYNC2LI1 disrupt cilia function and cause short rib polydactyly syndrome.
1018 *Nat Commun* **6**, 7092, doi:10.1038/ncomms8092 (2015).
1019 43 Tao, D. *et al.* Primary cilia support cartilage regeneration after injury. *Int J Oral Sci* **15**, 22,
1020 doi:10.1038/s41368-023-00223-6 (2023).
1021 44 Liu, X. *et al.* Numb positively regulates Hedgehog signaling at the ciliary pocket. *Nat Commun* **15**, 3365,
1022 doi:10.1038/s41467-024-47244-1 (2024).
1023 45 Allard, B. A. *et al.* Thm2 interacts with paralog, Thm1, and sensitizes to Hedgehog signaling in postnatal
1024 skeletogenesis. *Cell Mol Life Sci* **78**, 3743-3762, doi:10.1007/s00018-021-03806-w (2021).
1025 46 Cong, Q. *et al.* A self-amplifying loop of YAP and SHH drives formation and expansion of heterotopic
1026 ossification. *Sci Transl Med* **13**, doi:10.1126/scitranslmed.abb2233 (2021).

1027 47 Yuan, X., Liu, M., Cao, X. & Yang, S. Ciliary IFT80 regulates dental pulp stem cells differentiation by
1028 FGF/FGFR1 and Hh/BMP2 signaling. *International Journal of Biological Sciences* **15**, 2087-2099,
1029 doi:10.7150/ijbs.27231 (2019).
1030 48 Wu, F. *et al.* Discoidin domain receptor 2 is an important modulator of BMP signaling during heterotopic
1031 bone formation. *Bone Research* **13**, 7, doi:10.1038/s41413-024-00391-z (2025).
1032 49 Jou, V., Peña, S. M. & Lehoczky, J. A. Regeneration-specific promoter switching facilitates Mest
1033 expression in the mouse digit tip to modulate neutrophil response. *NPJ Regen Med* **9**, 32,
1034 doi:10.1038/s41536-024-00376-w (2024).
1035 50 Lu, W. *et al.* Hedgehog signaling regulates bone homeostasis through orchestrating osteoclast
1036 differentiation and osteoclast-osteoblast coupling. *Cell Mol Life Sci* **80**, 171, doi:10.1007/s00018-023-
1037 04821-9 (2023).
1038 51 Wang, Y. *et al.* TMEM216 promotes primary ciliogenesis and Hedgehog signaling through the SUFU-
1039 GLI2/GLI3 axis. *Sci Signal* **17**, eabo0465, doi:10.1126/scisignal.abo0465 (2024).
1040 52 Tang, R. *et al.* Stromal Stiffness-Regulated IGF2BP2 in Pancreatic Cancer Drives Immune Evasion via
1041 Sphingomyelin Metabolism. *Gastroenterology*, doi:10.1053/j.gastro.2025.03.019 (2025).
1042 53 Liu, J. *et al.* Macrophage sphingomyelin synthase 2 deficiency decreases atherosclerosis in mice. *Circ Res*
1043 **105**, 295-303, doi:10.1161/CIRCRESAHA.109.194613 (2009).
1044 54 Costantini, A. *et al.* Early-Onset Osteoporosis: Rare Monogenic Forms Elucidate the Complexity of
1045 Disease Pathogenesis Beyond Type I Collagen. *J Bone Miner Res* **37**, 1623-1641, doi:10.1002/jbmr.4668
1046 (2022).
1047 55 Hu, X. *et al.* Burn-induced heterotopic ossification from incidence to therapy: key signaling pathways
1048 underlying ectopic bone formation. *Cell Mol Biol Lett* **26**, 34, doi:10.1186/s11658-021-00277-6 (2021).
1049 56 Nunez, J. H. *et al.* Neutrophil and NETosis Modulation in Traumatic Heterotopic Ossification. *Ann Surg*
1050 **278**, e1289-e1298, doi:10.1097/SLA.0000000000005940 (2023).
1051 57 Wang, T. *et al.* IFT80 and TRPA1 cooperatively regulate bone formation by calcium signaling in response
1052 to mechanical stimuli. *Metabolism* **166**, 156159, doi:10.1016/j.metabol.2025.156159 (2025).
1053 58 Chen, M. *et al.* Noncanonical Wnt5a signaling regulates tendon stem/progenitor cells senescence. *Stem Cell*
1054 *Res Ther* **12**, 544, doi:10.1186/s13287-021-02605-1 (2021).
1055 59 Bi, Y. *et al.* Identification of tendon stem/progenitor cells and the role of the extracellular matrix in their
1056 niche. *Nat Med* **13**, 1219-1227 (2007).
1057 60 Wu, J. *et al.* Endothelial Cell-Derived Lactate Triggers Bone Mesenchymal Stem Cell Histone Lactylation
1058 to Attenuate Osteoporosis. *Adv Sci (Weinh)* **10**, e2301300, doi:10.1002/advs.202301300 (2023).
1059

1060 **Acknowledgments:** We thank Airu Zhu at Shanghai Bioprofile Technology Company. Ltd for
1061 her technical support in mass spectroscopy. Schematic diagrams (Figure 1a, 6a, 6b, and
1062 S7) were created with BioRender (https://www.biorender.com/).

1063 **Funding:** National Natural Science Foundation of China 82372434 (XHZ); National Natural
1064 Science Foundation of China 82302084 (HJ); National Natural Science Foundation of
1065 China 82402965 (RG)

1066 **Author contributions:** Conceptualization: HJ, XHZ; Methodology: BWL, JQZ; Investigation:
1067 BWL, YG; Visualization: BWL, ZLS; Funding acquisition: HJ, RG, XHZ; Project
1068 administration: HJ, XHZ; Supervision: JQZ, RG; Writing – original draft: BWL, YG;
1069 Writing – review & editing: HJ, XHZ

1070 **Competing interests:** Authors declare that they have no competing interests.

1071 **Data and materials availability:** The data that support the findings of this study are available
1072 from corresponding author upon reasonable request. Publicly available datasets were
1073 analyzed in this study, these can be found in Gene Expression Omnibus (GSE126060,
1074 GSE246445 and GSE233201) of National Center for Biotechnology Information.

1075 **Ethical approval:** All animal procedures were conducted in accordance with the guidelines of
1076 the Ethics Committee on Animal Experiments of the Naval Medical University.

1077 **Figures**

1078

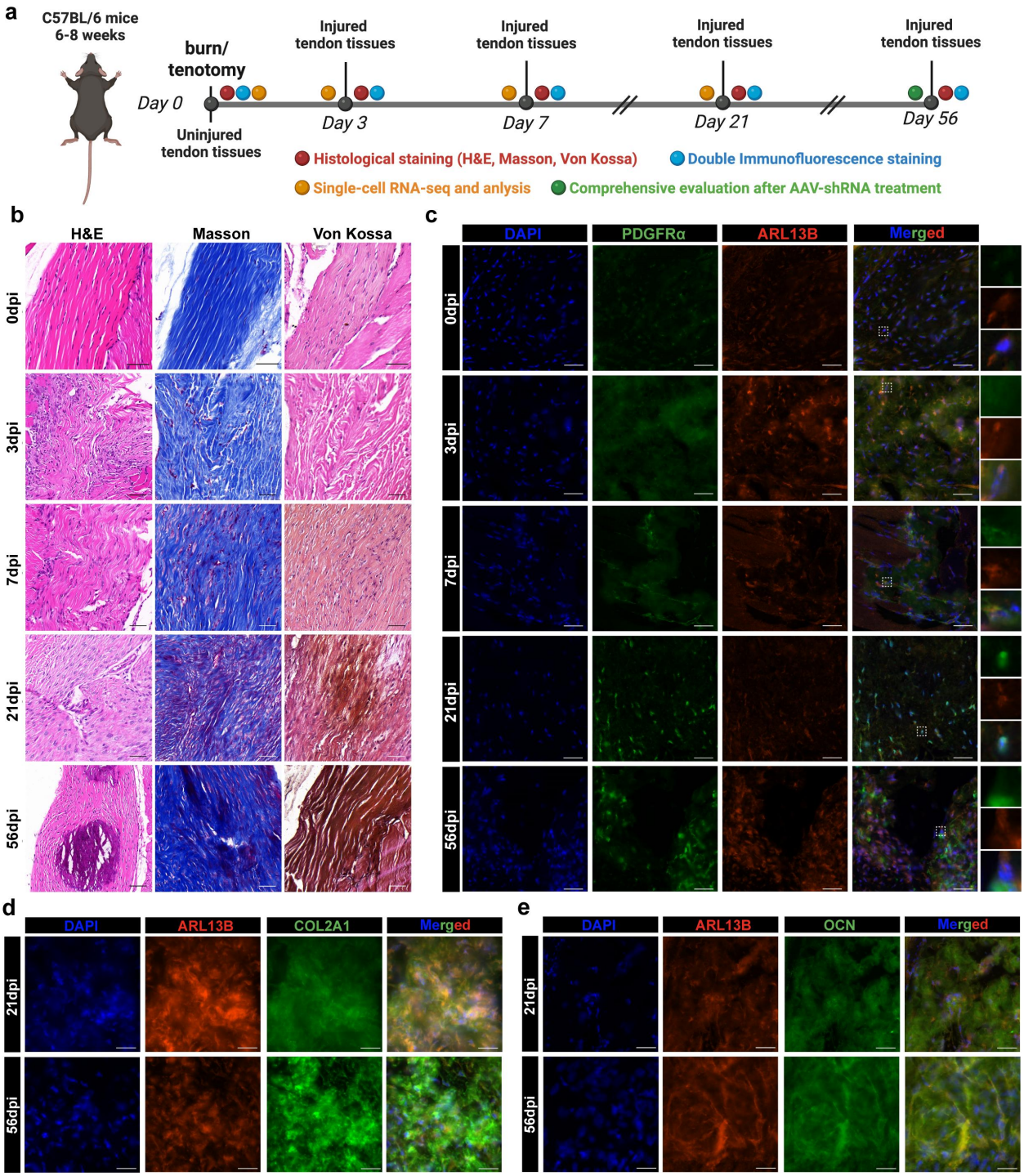

Figure 1. The number of primary cilia-positive cells increases during tHO formation. (a) Schematic diagram of the experimental workflow. (b) H&E, Masson trichrome, and Von Kossa staining of tHO tendon tissues collected from different time points after injury (scale bar 50 μm). (c) Immunofluorescence images of PDGFRα (green) and ARL13B (red) at different time points during tHO development. DAPI staining indicates nuclei (blue), scale bar 30 μm. (d) Immunofluorescence images of COL2A1 (green) and ARL13B (red) in injured sites at 21 and 56 days after

1085 tHO. DAPI staining indicates nuclei (blue), scale bar 30 μm. (d) Immunofluorescence images of OCN (green) and
1086 ARL13B (red) in injured sites at 21 and 56 days after tHO. DAPI staining indicates nuclei (blue), scale bar 30 μm.
1087

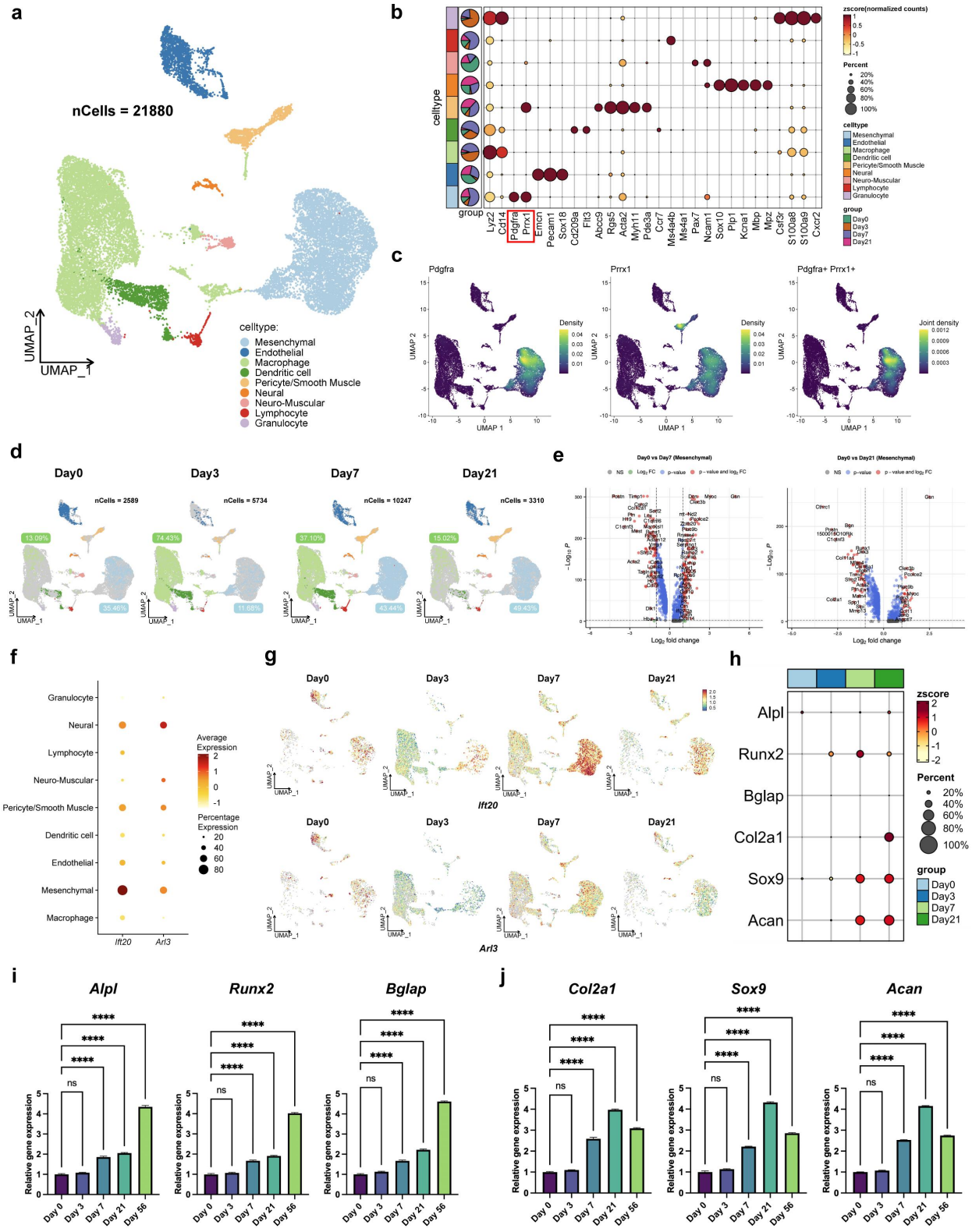

Figure 2. scRNA-seq indicated the role of stem/progenitor cells and ciliary genes in tHO development. (a) UMAP plot of nine clusters identified in 21880 cells in total of tHO injured site. (b) Bubble plot shows the high variable marker genes of each cluster. The red box highlights Pdgfra and Prrx1 as markers for the Mesenchymal

1092 cluster. (c) The expression density of Pdgfra+, Prrx1+, and Pdgfra+Prrx1+ cells in each cluster are shown by UMAP
1093 plot. The purple-to-yellow gradient signifies a progressive increase in expression levels. (d) UMAP plot of nine
1094 clusters with single cells grouped by different time points (Day 0 ,3, 7, 21) during tHO demonstrates the trend of
1095 changes in cell composition. (e) The volcano plot visualizes the differential expressed genes in the Mesenchymal
1096 subcluster at Day 7 (left) or Day 21 (right) compared to the Day 0 group. (f) The dot plot visualizes the different
1097 expression of *Ift20* and *Arl3* in nine clusters. (g) UMAP plot shows the expression of *Ift20* (upper) and *Arl3* (lower)
1098 at different time points (Day 0 ,3, 7, 21) during tHO development. (h) Bubble plot shows the different expression of
1099 osteogenic and chondrogenic genes in four groups during tHO development. (i) qPCR showed relative osteogenesis-
1100 related genes (*Alpl, Runx2,* and *Bglap*) mRNA expression in different time points (Day 0, 3, 7, 21) during tHO
1101 development. (j) qPCR showed relative chondrogenesis-related genes (*Col2a1, Sox9,* and *Acan*) mRNA expression
1102 in different time points (Day 0, 3, 7, 21) during tHO development. Data are presented as means ± SD of three
1103 independent assays. Statistical analyses were performed by one-way ANOVA analyses with Tukey's post hoc test
1104 for multiple comparisons. ****$P < 0.001$; ns, $P > 0.05$.
1105

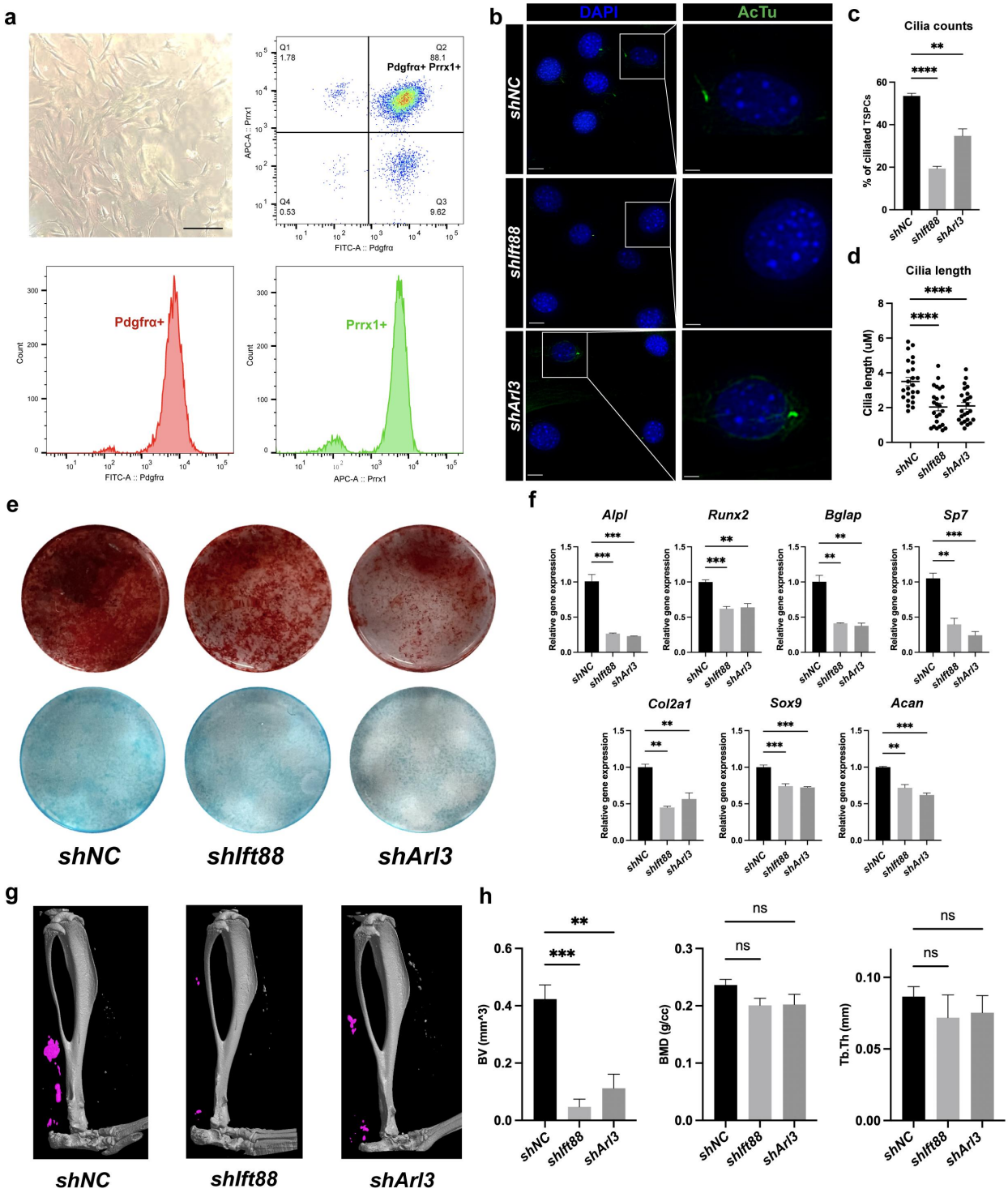

Figure 3. Primary cilia dysfunction impairs TSPCs osteochondrogenesis and ectopic bone formation. (a) Fibroblast-like TSPCs extracted from mice for subsequent experiments (scale bar 100 μm) and flow cytometry analysis of the expression of Pdgfra and Prrx1 (stem/progenitor cell surface markers) on TSPCs. (b) Immunofluorescence images of AcTu (green) mark the cilia in *shNC, shIFT88,* and *shARL3* TSPCs. DAPI staining indicates nuclei (blue), scale bar 30 μm (left) and 10 μm (right). (c) Cilia counts (qualified by the percentage of

1112 ciliated TSPCs) in TSPCs with or without *shIFT88* or *shARL3* treatment. (d) Cilia length in TSPCs with or without
1113 *shIFT88* or *shARL3* treatment (n= 25/group). (e) Representative images of alizarin red staining (upper) and alcian
1114 blue staining (lower) in TSPCs with or without *shIFT88* or *shARL3* treatment during in vitro osteogenic or
1115 chondrogenic differentiation. (f) qPCR showed relative osteogenesis-related genes (*Alpl, Runx2, Bglap, and Sp7*)
1116 and chondrogenesis-related genes (*Col2a1, Sox9, and Acan*) mRNA expression in TSPCs with or without *shIFT88*
1117 or *shARL3* treatment after during in vitro osteogenic or chondrogenic differentiation. (g) Micro-CT images show
1118 tHO of lower limbs among *shNC, shIFT88,* and *shARL3* groups (n= 4/group). (h) Bone volume (BV, mm^3), bone
1119 mineral density (BMD, g/cc), and Tb.Th (trabecular thickness, mm) are quantified. Independent experiments (n=
1120 4/group) were performed for measurements. Data are presented as means ± SD of three independent assays.
1121 Statistical analyses were performed by one-way ANOVA analyses with Tukey's post hoc test for multiple
1122 comparisons. *P < 0.05; **P < 0.01; ***P < 0.005; ****P < 0.001; ns, P > 0.05.
1123

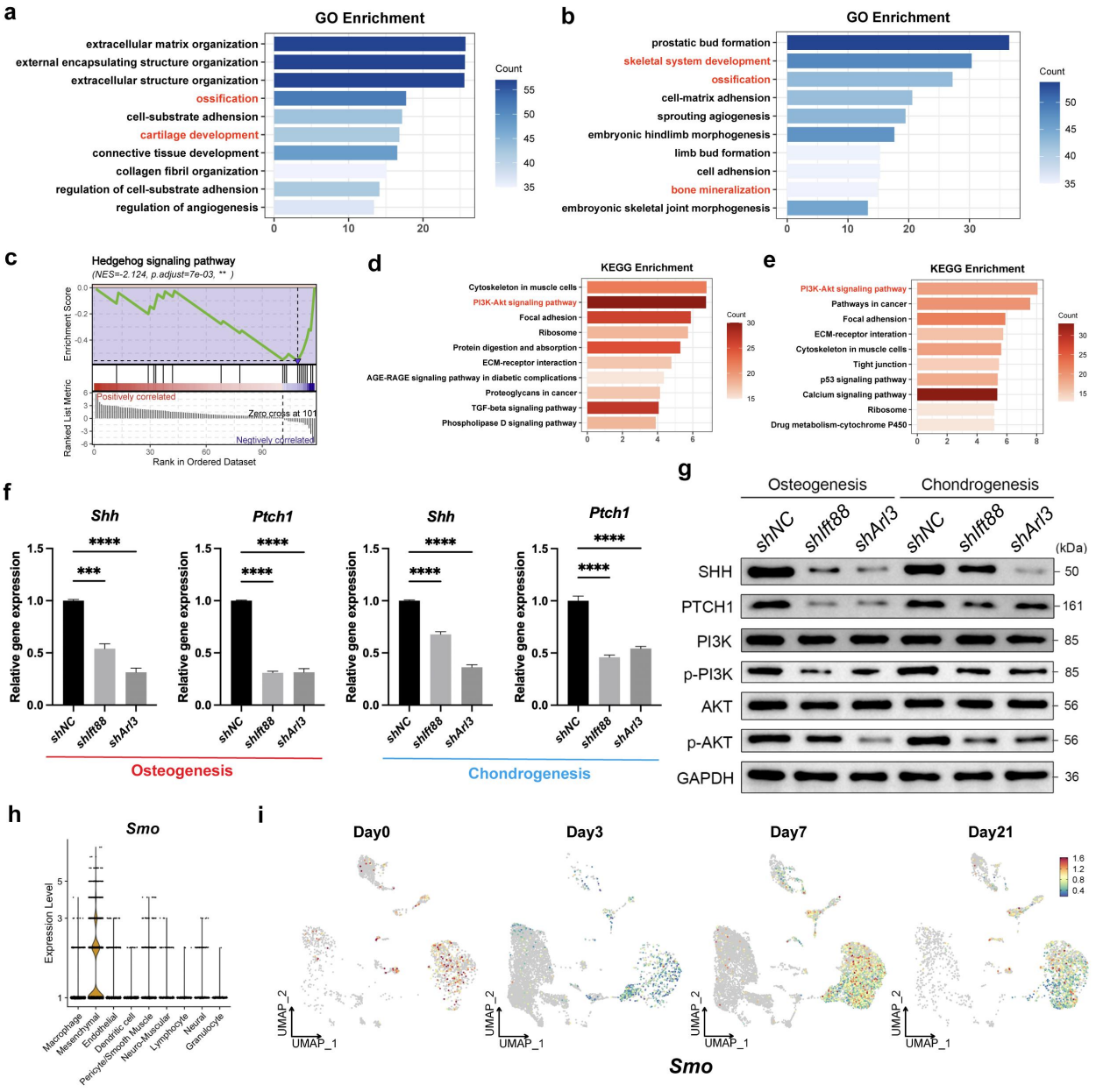

Figure 4. TSPCs ciliary Hh and PI3K-Akt signaling are involved in tHO progression. (a) GO enrichment analysis of differential expressed genes in tHO mice injured site shows top 10 enriched biological processes that are important for tHO. (b) GO enrichment analysis of differential expressed genes in TSPCs treated with *shIft88* shows top 10 enriched biological processes. (c) GSEA enrichment of TSPCs treated with *shIft88* compared with *shNC*. The enriched pathway with the absolute value of normalized enrichment score (NES) greater than 1 and adjusted P-value less than 0.05 was considered significant. (d) KEGG enrichment analysis of differential expressed genes in Mesenchymal subcluster of tHO injured site identified by scRNA-seq shows top 10 enriched pathways. (e) KEGG enrichment analysis of differential expressed genes in TSPCs treated with *shIft88* showed top enriched pathways. (f) qPCR showed relative Hh signaling genes (Shh, Ptch1) mRNA expression in TSPCs with or without *shIft88* or *shARL3* treatment during in vitro osteogenic or chondrogenic differentiation. (g) Western blot showed Hh signaling

1135 (SHH, PTCH1) and PI3K-Akt signaling (PI3K, p-PI3K, AKT, p-AKT) protein expression levels in TSPCs with or
1136 without *shIFT88* or *shARL3* treatment during in vitro osteogenic or chondrogenic differentiation. (h) The expression
1137 level of *Smo* in each cluster are shown by violin plot. (i) UMAP plot shows the expression of *Smo* at different time
1138 points (Day0 ,3, 7, 21) during tHO development. Data are presented as means ± SD of three independent assays.
1139 Statistical analyses were performed by one-way ANOVA analyses with Tukey's post hoc test for multiple
1140 comparisons. ***$P < 0.005$; ****$P < 0.001$
1141

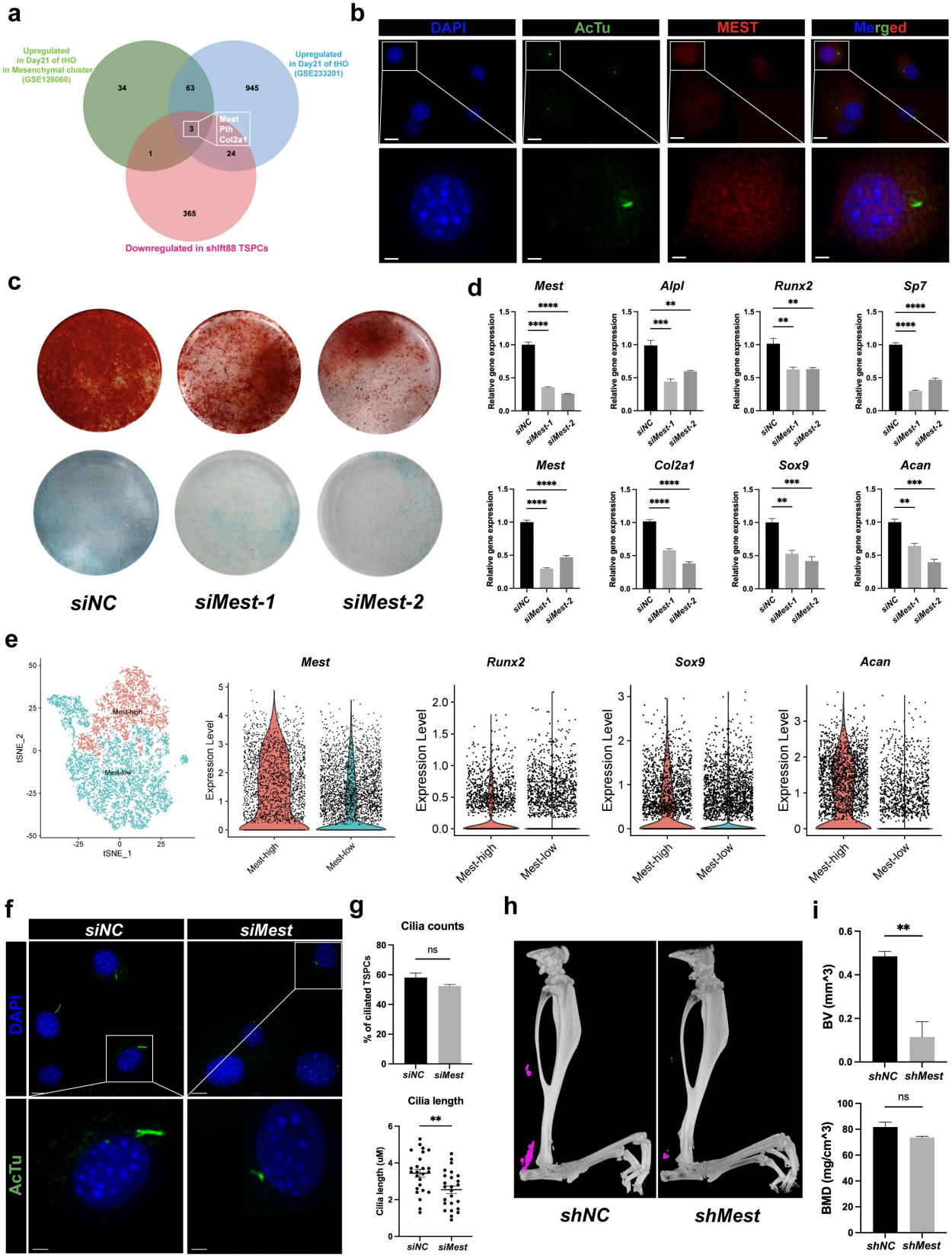
a
Upregulated in Day21 of tHO in Mesenchymal cluster (GSE126060)
Upregulated in Day21 of tHO (GSE233201)
Downregulated in shIft88 TSPCs
34
63
945
3
1
24
365
Mest
Pth
Col2a1
b
DAPI
AcTu
MEST
Merged
c
siNC
siMest-1
siMest-2
d
Mest
Alpl
Runx2
Sp7
Col2a1
Sox9
Acan
Relative gene expression
e
Mest-high
Mest-low
tSNE_1
tSNE_2
Expression Level
f
siNC
siMest
DAPI
AcTu
g
Cilia counts
% of ciliated TSPCs
ns
Cilia length
Cilia length (uM)
h
shNC
shMest
i
BV (mm^3)
BMD (mg/cm^3)

1142

1143 **Figure 5. MEST modulates TSPCs cilia length and osteochondrogenesis in tHO.** (a) Venn diagram shows the
1144 common differential expressed genes among three gene sets and identified MEST, PTN, COL2A1 as the key genes.
1145 (b) Immunofluorescence images of AcTu (green) and MEST (red) in TSPCs. DAPI staining indicates nuclei (blue),
1146 scale bar 30 μm (upper) and 10 μm (lower). (c) Representative images of alizarin red staining (upper) and alcian
1147 blue staining (lower) in TSPCs with or without *siMest* treatment during in vitro osteogenic or chondrogenic
1148 differentiation. (d) qPCR shows relative *Mest* and osteogenesis-related (*Alpl, Runx2, Bglap*) or chondrogenesis-
1149 related genes (*Col2a1, Sox9, Acan*) mRNA expression in TSPCs with or without *siMest* treatment during in vitro
1150 osteogenic or chondrogenic differentiation. (e) tSNE map shows Mest-high and Mest-low subclusters divided from
1151 Mesenchymal cluster. The expression level of *Mest, Runx2, Sox9*, and *Acan* in Mest-high and Mest-low subclusters
1152 were visualize by violin plots. (f) Immunofluorescence images of AcTu (green) mark the cilia of TSPCs. DAPI
1153 staining indicates nuclei (blue), scale bar 30 μm (upper) and 10 μm (lower). (g) Cilia counts (qualified by ciliated
1154 TSPCs proportion) and cilia length (n= 25/group) in the *siNC* and *siMest* group. (h) Micro-CT images show tHO of
1155 lower limbs in *shNC* and *shMest* groups. (i) Quantification of tHO degree by bone volume (BV, mm^3) and bone
1156 mineral density (BMD, mg/cm^3). Independent experiments (n= 4/group) were performed for measurements. Data
1157 are presented as means ± SD of three independent assays. Statistical analyses were performed by Student's t-test for
1158 two-group comparison and one-way ANOVA analyses with Tukey's post hoc test for multiple comparisons. *P <
1159 0.05; **P < 0.01; ***P < 0.005; ****P < 0.001; ns, P > 0.05.
1160

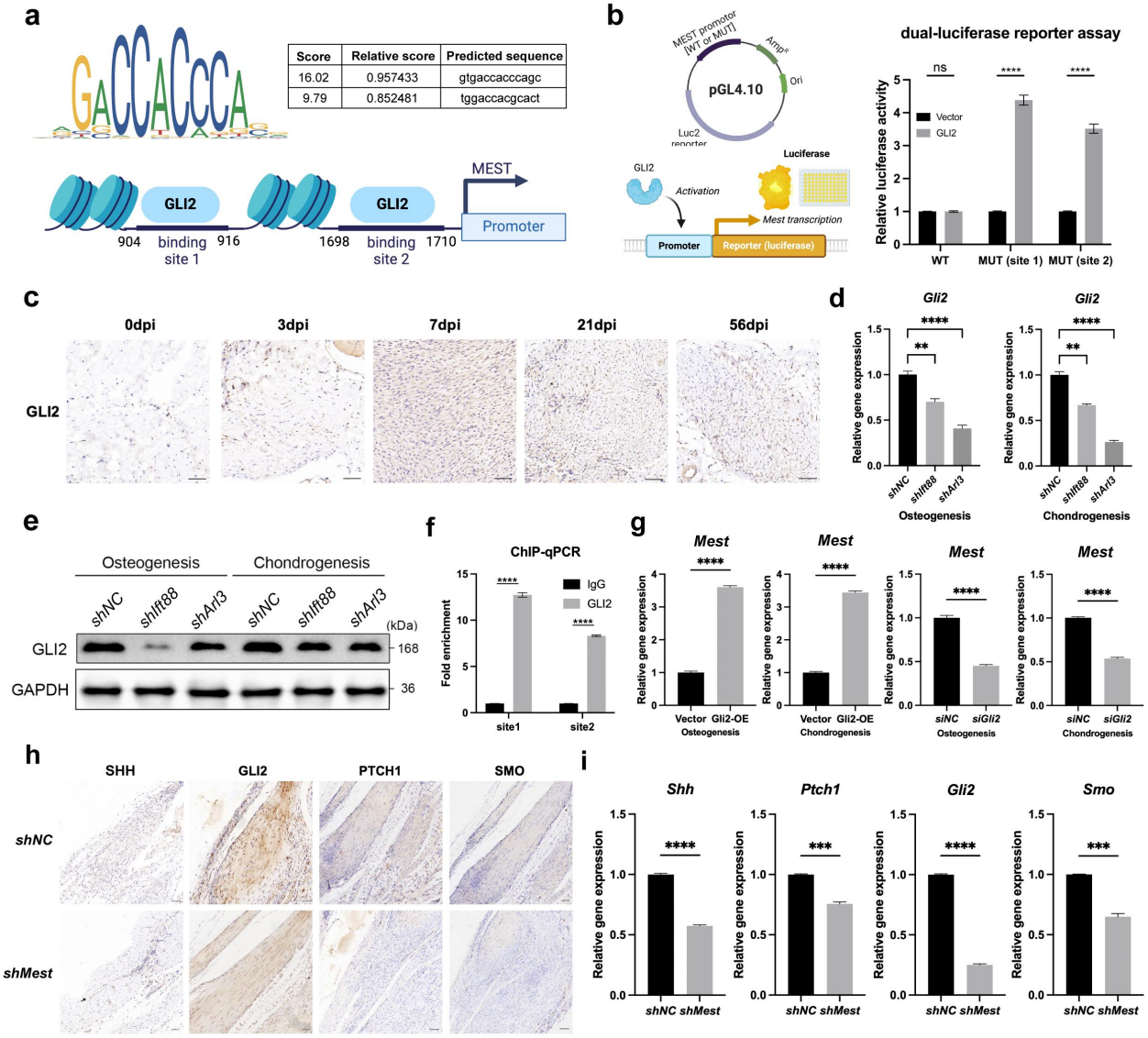

Figure 6. GLI2 binds to the MEST promoter to activate its transcription via Hh signaling. (a) The sequence logo of GLI2 transcription factor and two potential binding sites of the GLI2 transcription factor on the MEST promoter region predicted by the JASPAR database. (b) The luciferase reporter assay using pGL4.10 as vector showed that GLI2 can bind to the MEST promoter at both site 1 and 2. (c) Immunohistochemistry images demonstrated GLI2 in tHO tendon tissues at different time post injury (scale bar 100 μm). (d) qPCR shows relative *Gli2* mRNA expression in TSPCs with or without *shIft88* or *shARL3* treatment during in vitro osteogenic or chondrogenic differentiation. (e) Western blot shows GLI2 protein expression levels in TSPCs with or without *shIFT88* or *shARL3* treatment during in vitro osteogenic or chondrogenic differentiation. (f) ChIP-qPCR shows GLI2 can binds to both the site 1 and site 2 of the MEST promoter region. (g) qPCR showed relative Mest mRNA expression in TSPCs with or without Gli2-OE or *siGli2* treatment during in vitro osteogenic or chondrogenic differentiation. (h) Immunohistochemistry images demonstrated SHH, GLI2, PTCH1, and SMO expression in tHO tendon tissues with *shNC* or *shMest* treatment after injury (scale bar 150 μm). (i) qPCR shows relative *Shh, Ptch1,*

1174 *Gli2,* and *Smo* mRNA expression in tHO tendon tissues with *shNC* or *shMest* treatment after injury. Data are
1175 presented as means ± SD of three independent assays. Statistical analyses were performed by Student's t-test for
1176 two-group comparison and one-way ANOVA analyses with Tukey's post hoc test for multiple comparisons. **P <
1177 0.01; ***P < 0.005; ****P < 0.001; ns, P > 0.05.
1178

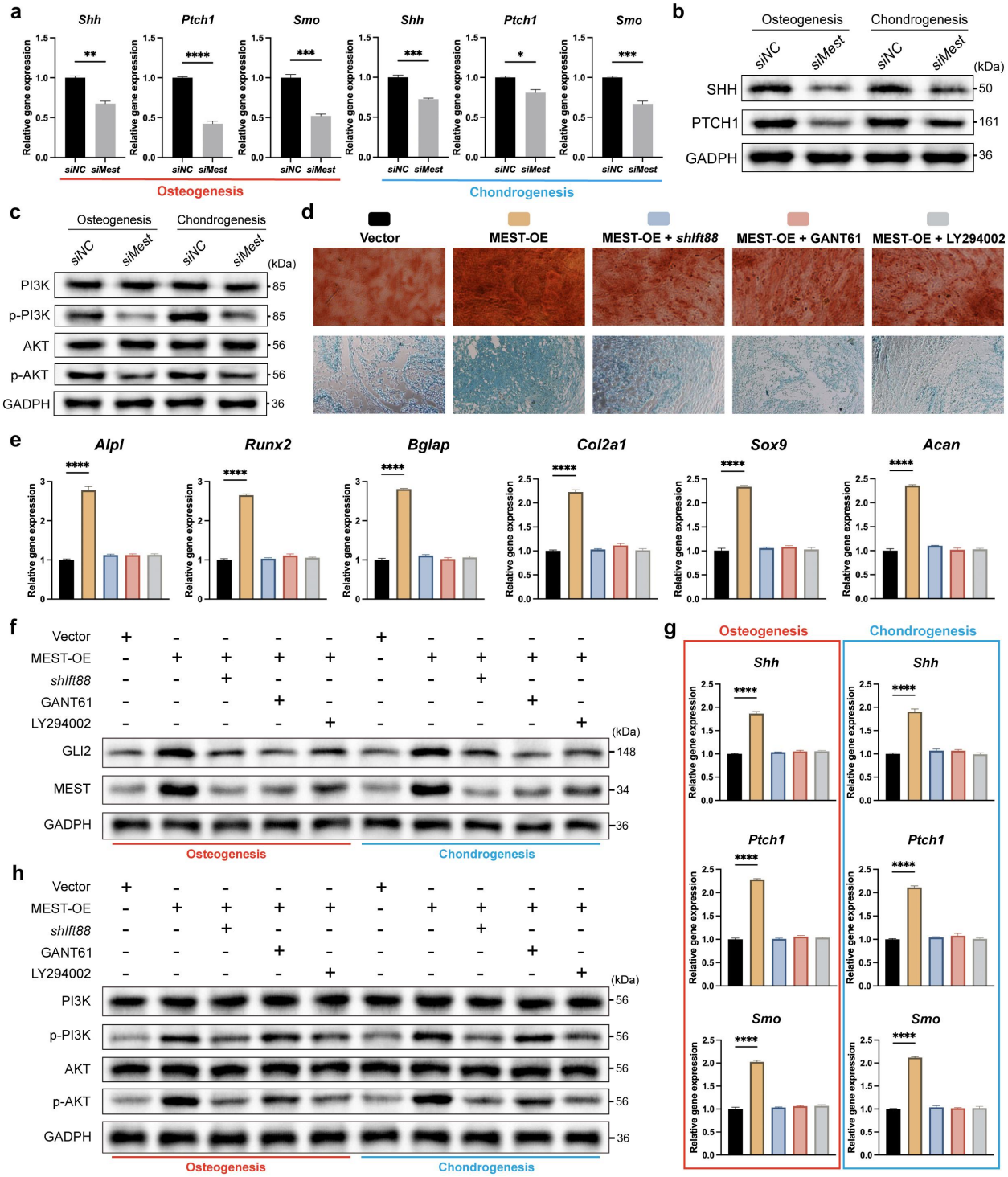

Figure 7. MEST enhances TSPCs osteochondrogenesis through Hh and PI3K-Akt signaling. (a) qPCR showed relative Hh signaling genes (*Shh, Ptch1, and Smo*) mRNA expression in TSPCs with or without *siMest* treatment during in vitro osteogenic or chondrogenic differentiation. (b) Western blot shows Hh signaling (SHH, PTCH1) protein expression levels in TSPCs with or without *siMest* treatment during in vitro osteogenic or chondrogenic differentiation. (c) Western blot showed PI3K-Akt signaling (PI3K, p-PI3K, AKT, p-AKT) protein expression levels

1185 in TSPCs with or without *siMest* treatment during in vitro osteogenic or chondrogenic differentiation. (d)
1186 Representative images of alizarin red staining (upper) and alcian blue staining (lower) in TSPCs during in vitro
1187 osteogenic (upper) and chondrogenic (lower) differentiation in Vector, MEST-OE, MEST-OE + *shIft88*, MEST-OE
1188 + GANT61, and MEST-OE + LY294002 treated groups. (e) qPCR showed relative osteogenesis-related genes (*Alpl,*
1189 *Runx2*, *Bglap*) and chondrogenesis-related genes (*Sox9, Col2a1, Acan*) mRNA expression after in vitro TSPCs
1190 osteogenic or chondrogenic differentiation in five groups. (f) Western blot showed GLI2 and MEST protein
1191 expression levels in TSPCs under different treatment during in vitro osteogenic or chondrogenic differentiation. (g)
1192 qPCR showed relative Hh signaling genes (*Shh, Ptch1, and Smo*) mRNA expression in TSPCs under different
1193 treatment during in vitro osteogenic or chondrogenic differentiation. (h) Western blot showed PI3K-Akt signaling
1194 (PI3K, p-PI3K, AKT, p-AKT) protein expression levels in TSPCs under different treatment during in vitro
1195 osteogenic or chondrogenic differentiation. Data are presented as means ± SD of three independent assays.
1196 Statistical analyses were performed by Student's t-test for two-group comparison and one-way ANOVA analyses
1197 with Tukey's post hoc test for multiple comparisons. *P < 0.05; **P < 0.01; ***P < 0.005; ****P < 0.001.
1198

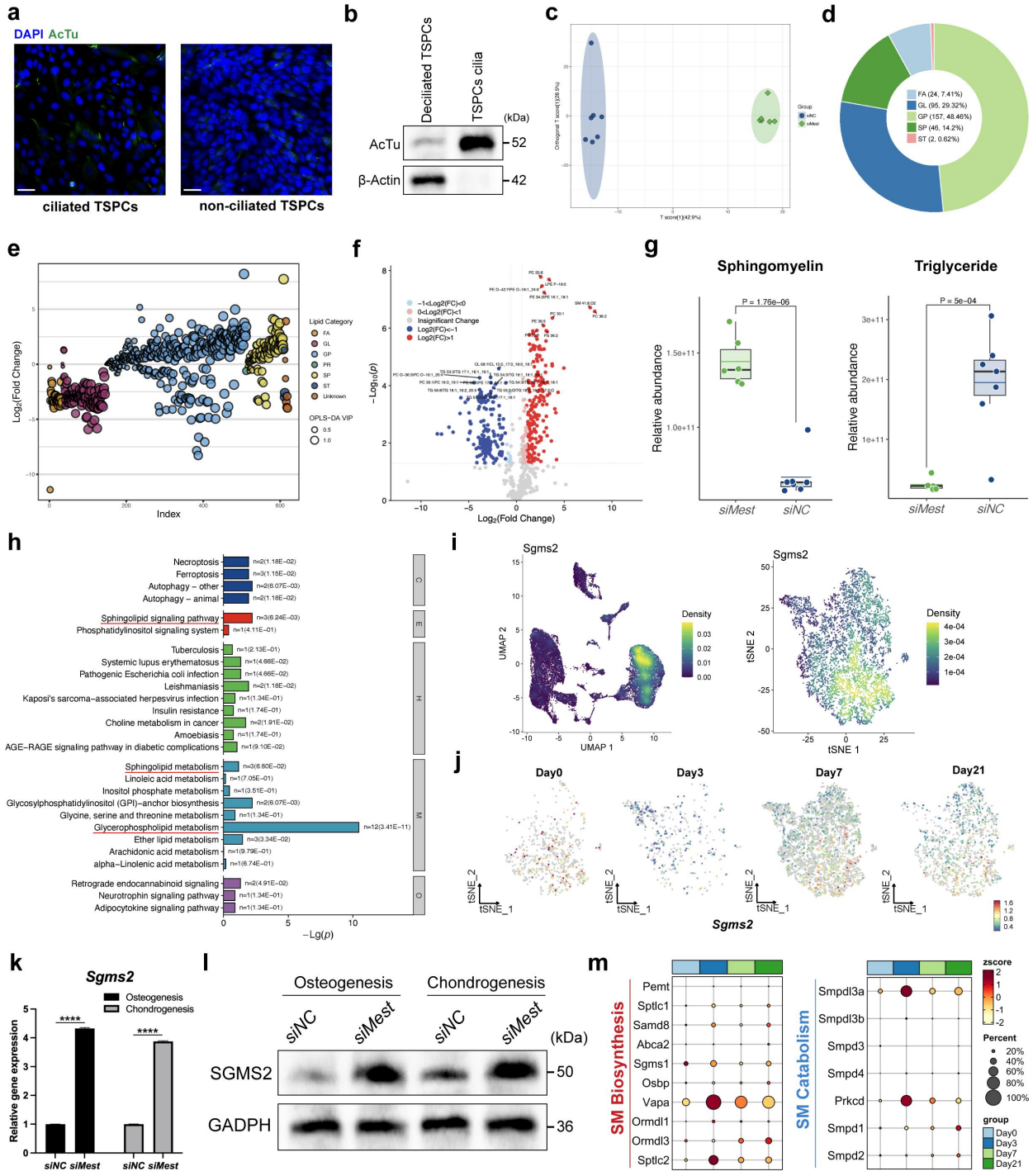

Figure 8. MEST regulates ciliary sphingomyelin metabolism in TSPCs. (a) Immunofluorescence images of AcTu (green) marked cilia in ciliated and non-ciliated mouse primary TSPCs after cilia isolation. DAPI staining indicates nuclei (blue). scale bar 100 µm. (b) Western blot analysis of extracted TSPCs cilia lysates and non-ciliated TSPCs. (c) OPLS-DA plot shows the differences between *siNC* (blue, n= 7) and *siMest* (green, n= 6) groups. (d) Circular diagram of the classification statistics of differential lipids. (e) Bubble chart of lipid classification. The horizontal axis represents the quantity range of lipids, and the vertical axis represents the logarithmic transformation

of fold change. Each circle represents a lipid substance. The larger the circle, the higher the variable importance. Different colors represent the primary classification, and lipids of the same classification are arranged together. (f) The volcano plot visualizes the differential expressed lipids in *siMest* group compared to the *siNC* group. Differential expressed lipids are visualized as red (upregulated) or blue (downregulated) bubbles, identified by expression fold-change and p-value. (g) Relative abundance of sphingomyelin and triglyceride are significantly different in *siMest* and *siNC* group. (h) KEGG enrichment analysis of differential expressed lipids between *siMest* and *siNC* group (C: cellular processes; E: environmental information processing; H: human diseases; M: metabolism; O: organismal systems). (i) The expression density of *Sgms2* in each cluster (left) and in Mesenchymal subcluster (right) are shown by UMAP plot. (j) UMAP plot shows the expression of *Sgms2* in Mesenchymal subcluster at different time points (Day0 ,3, 7, 21) during tHO development. (k) qPCR shows relative *Sgms2* mRNA expression in TSPCs with or without *siMest* treatment during in vitro osteogenic or chondrogenic differentiation. (l) Western blot shows SGMS2 protein expression levels in TSPCs with or without *siMest* treatment during in vitro osteogenic or chondrogenic differentiation. (m) Bubble plot shows the different expression of SM biosynthesis (red) or catabolism (blue) related genes at different time points (Day 0 ,3, 7, 21) during tHO development. Data are presented as means ± SD of three independent assays. Statistical analyses were performed by Student's t-test for two-group comparison. ****$P < 0.001$.

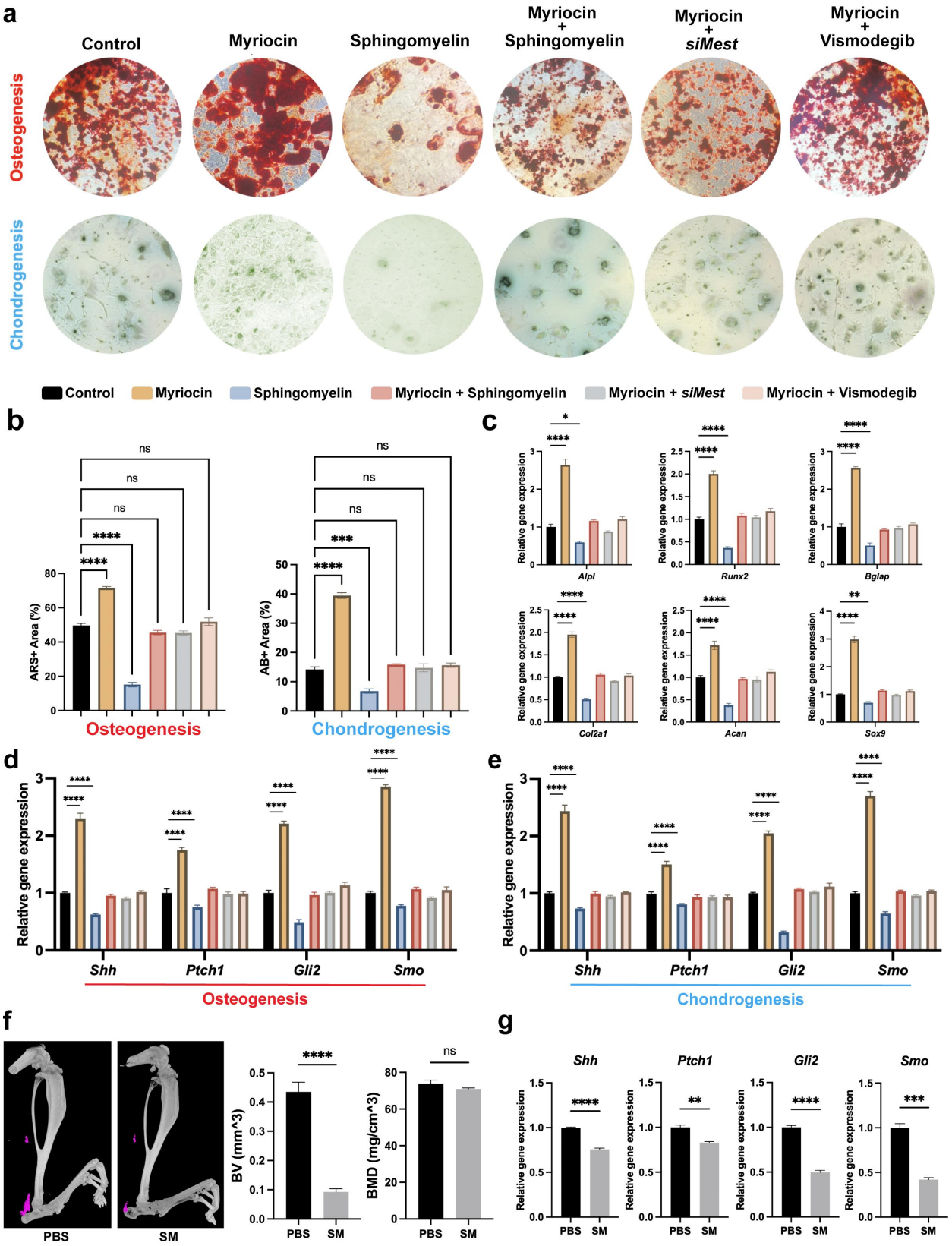
a
Control
Myriocin
Sphingomyelin
Myriocin + Sphingomyelin
Myriocin + siMest
Myriocin + Vismodegib
Osteogenesis
Chondrogenesis
Control
Myriocin
Sphingomyelin
Myriocin + Sphingomyelin
Myriocin + siMest
Myriocin + Vismodegib
b
ARS+ Area (%)
AB+ Area (%)
Osteogenesis
Chondrogenesis
c
Relative gene expression
Alpl
Runx2
Bglap
Col2a1
Acan
Sox9
d
Relative gene expression
Shh
Ptch1
Gli2
Smo
Osteogenesis
e
Relative gene expression
Shh
Ptch1
Gli2
Smo
Chondrogenesis
f
PBS
SM
BV (mm^3)
BMD (mg/cm^3)
g
Shh
Ptch1
Gli2
Smo
Relative gene expression

1223

1224 **Figure 9. Targeting ciliary sphingomyelin in TSPCs alleviates tHO via Hh signaling.** (a) Representative images
1225 of alizarin red staining (upper) and alcian blue staining (lower) in TSPCs during in vitro osteogenic (upper) and
1226 chondrogenic (lower) differentiation in control, myriocin, sphingomyelin, myriocin + sphingomyelin, myriocin +
1227 siMest, and myriocin + vismodegib treated groups. (b) Quantification of the percentages of alizarin red positive
1228 (ARS+) and alcian blue positive (AB+) areas in six groups. (c) qPCR showed relative osteogenesis-related genes
1229 *(Alpl, Runx2, Bglap*) and chondrogenesis-related genes (*Sox9, Col2a1, Acan*) mRNA expression after in vitro
1230 TSPCs osteogenic (upper) or chondrogenic (lower) differentiation in six groups. (d) qPCR showed relative Hh
1231 signaling genes (*Shh, Ptch1, Gli2, Smo*) mRNA expression after in vitro TSPCs osteogenic differentiation in six
1232 groups. (e) qPCR showed relative Hh signaling genes (*Shh, Ptch1, Gli2, Smo*) mRNA expression after in vitro
1233 TSPCs chondrogenic differentiation in six groups. (f) Micro-CT images show tHO of lower limbs between 1X PBS
1234 and sphingomyelin (SM) treated groups. Quantification of tHO degree by bone volume (BV, mm^3) and bone
1235 mineral density (BMD, mg/cm^3). Independent experiments (n= 4/group) were performed for measurements. (g)
1236 qPCR shows relative *Shh, Ptch1, Gli2,* and *Smo* mRNA expression in tHO mice injured site with PBS or SM
1237 treatment. Data are presented as means ± SD of three independent assays. Statistical analyses were performed by
1238 Student's t-test for two-group comparison and one-way ANOVA analyses with Tukey's post hoc test for multiple
1239 comparisons. *P < 0.05; **P < 0.01; ***P < 0.005; ****P < 0.001; ns, P > 0.05.
1240

Figure 10. scRNA-seq analysis of the injured tibial muscle from *Nse-Bmp4* tHO mice. (a) UMAP plot of nine clusters identified in 45287 cells in total of *Nse-Bmp4* mice injured muscle. (b) The percentage of each annotated cell type in four groups and its trend. (c) UMAP plot shows the expression density of *Mest* in each cluster. (d) UMAP plot shows the expression of *Mest* from *Nse-Bmp4* mice injured muscle in different groups during tHO development at single-cell levels. (e) Heatmap of the top 10 higher variable genes of four groups in MSC lineages cluster. (f) GO and KEGG enrichment analyses of differential expressed genes (DEGs) in *Nse-Bmp4* mice muscle at

1249 7 days post injury shows top 10 enriched functions and pathways that are important for tHO. (g) Venn plot shows
1250 the 13 common genes between cilia genes and DEGs of Day 7 group in MSC lineages cluster. (h) The dot plot
1251 visualizes the different expression of 13 common genes in nine clusters. (i) Bubble plot shows the different
1252 expression of 13 common genes in four groups of MSC lineages cluster.
1253

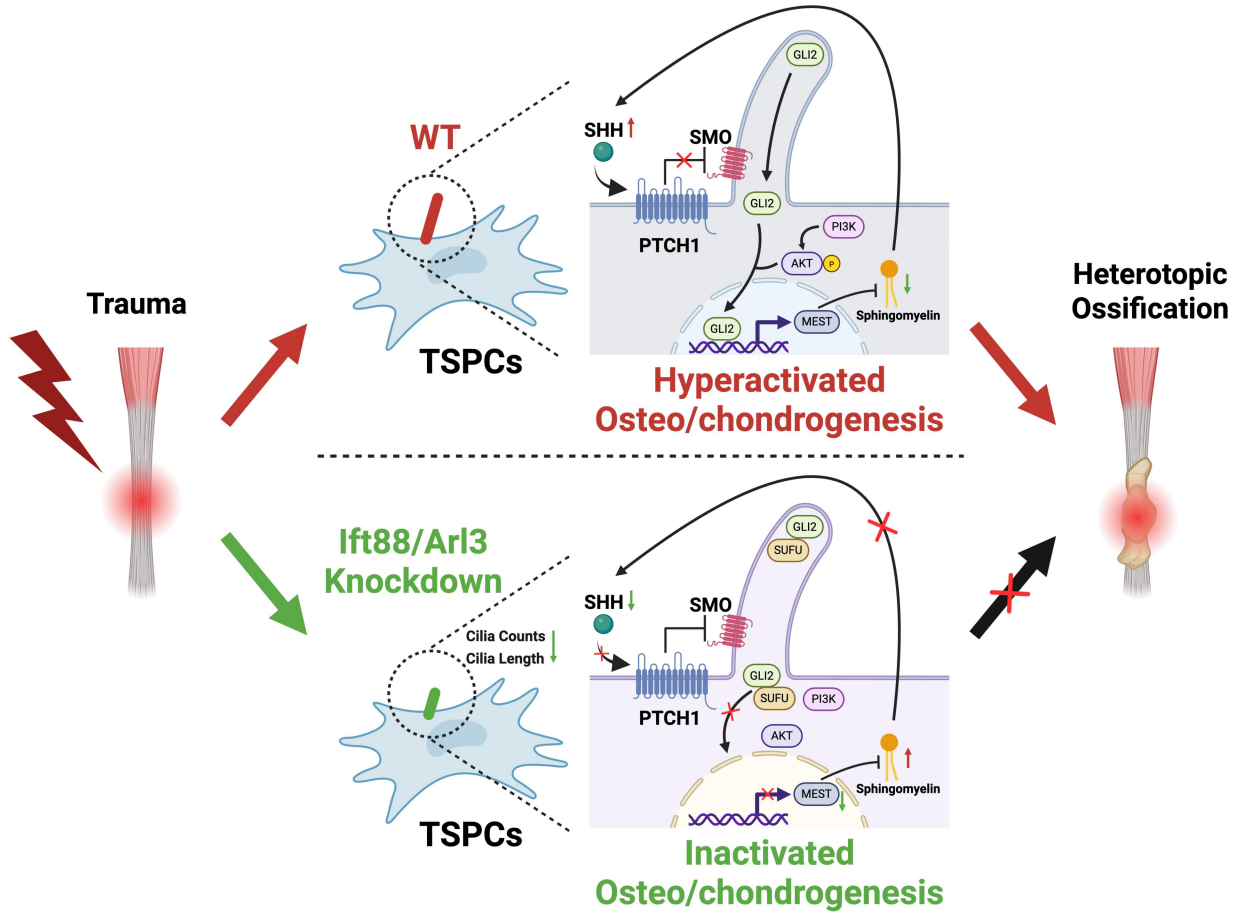

Figure 11. Schematic diagram of the study. SHH is unregulated within the primary cilia of TSPCs after trauma, activating the Hh signaling through its interaction with PTCH1 and SMO receptors. Subsequently, the GLI2 transcription factor activated and translocated to the nucleus, where it promotes the expression of the MEST gene. Concurrently, the phosphorylation levels of PI3K and AKT are enhanced. The upregulation of MEST expression inhibits sphingomyelin synthesis and leads to a reduction in sphingomyelin levels within the cilia, further amplifying the activation of the ciliary Hh signaling. This positive feedback loop dramatically enhances the osteogenic and chondrogenic differentiation potential of TSPCs, resulting in localized ectopic bone deposition and tHO. Conversely, when the ciliary genes Ift88 and Arl3 are knocked down in TSPCs, the production of SHH ligands is markedly reduced. Thus, SMO is inhibited by PTCH1, preventing the activation of GLI2. Additionally, the phosphorylation of PI3K and AKT is suppressed. The reduction in MEST expression subsequently increases the sphingomyelin within the cilia, which further inhibits the ciliary Hh signaling. As a result, the osteogenic and chondrogenic differentiation capacity of TSPCs is significantly diminished, thereby alleviating the occurrence and development of tHO.